Activation of Pro-uPA Is Critical for Initial Escape from the Primary Tumor and Hematogenous Dissemination of Human Carcinoma Cells[1,2]

Erin M. Bekes*, Elena I. Deryugina*, Tatyana A. Kupriyanova*, Ewa Zajac*, Kenneth A. Botkjaer[†], Peter A. Andreasen[†] and James P. Quigley*

*Department of Cell Biology, The Scripps Research Institute, La Jolla, CA, USA; [†]Department of Molecular Biology, Aarhus University, Aarhus, Denmark

Abstract

Urokinase-type plasminogen activator (uPA) and plasmin have long been implicated in cancer progression. However, the precise contributions of the uPA/plasmin system to specific steps involved in cancer cell dissemination have not been fully established. Herein, we have used a highly disseminating variant of the human PC-3 prostate carcinoma cell line, PC-hi/diss, as a prototype of aggressive carcinomas to investigate the mechanisms whereby pro-uPA activation and uPA-generated plasmin functionally contribute to specific stages of metastasis. The PC-hi/diss cells secrete and activate significant amounts of pro-uPA, leading to efficient generation of plasmin in solution and at the cell surface. In a mouse orthotopic xenograft model, treatment with the specific pro-uPA activation–blocking antibody mAb-112 significantly inhibited local invasion and distant metastasis of the PC-hi/diss cells. To mechanistically examine the uPA/plasmin–mediated aspects of tumor cell dissemination, the anti–pro-uPA mAb-112 and the potent serine protease inhibitor, aprotinin, were used in parallel in a number of *in vivo* assays modeling various rate-limiting steps in early metastatic spread. Our findings demonstrate that, by generating plasmin, activated tumor-derived uPA facilitates early stages of PC-hi/diss dissemination, specifically the escape from the primary tumor and tumor cell intravasation. Moreover, through a series of *in vitro* and *in vivo* analyses, we suggest that PC-hi/diss–invasive escape and dissemination may be enhanced by cleavage of stromal fibronectin by uPA-generated plasmin. Together, our findings point to inhibition of pro-uPA activation at the apex of the uPA/plasmin cascade as a therapy-valid approach to control onset of tumor escape and ensuing metastatic spread.

Introduction

Increased levels and activity of proteolytic enzymes have been linked to enhanced motility, invasion, and metastasis of tumor cells [1,2]. Specifically, the serine protease urokinase-type plasminogen activator (uPA) is often elevated in aggressive cancers, especially in prostate cancer [3–6]. In normal tissues, uPA is tightly regulated at the level of proenzyme activation as well as at the level of enzyme activity. However, during cancer invasion and metastasis this tight control of uPA system is dysregulated.

The uPA molecule is secreted as an inactive, single-chain zymogen, pro-uPA, which must be proteolytically converted into an active enzyme before it can exert its major biologic function, that is, convert plasminogen to the active plasmin. In a reciprocal fashion, plasmin activates the single-chain pro-uPA through hydrolysis of the Lys_{158}-Ile_{159} bond, yielding two, A and B chains, which remain covalently

linked by a disulfide bond [7–10]. Although a secreted protease, uPA can be tethered to the cell surface through binding of its growth factor–like domain to the GPI-anchored cell surface receptor, uPAR [11,12]. Both pro-uPA and activated uPA bind uPAR with similar affinities; however, cell surface–bound uPA is significantly more potent in the catalytic conversion of plasminogen to plasmin [13]. Plasmin (ogen) also can be localized to the cell surface by binding to C-terminal lysine residues of several membrane proteins, including annexin II and Plg-RKT [14,15]. Furthermore, cell surface–bound plasmin is protected from inhibition by circulating inhibitors, thereby enhancing its cell-associated functions [16]. The pericellular localization of both uPA and plasmin activity is believed to facilitate cell invasion during wound healing and tumor progression. Once activated by uPA, plasmin has a broad substrate repertoire. Whereas the canonical function of active plasmin is fibrin clot lysis, plasmin can also cleave several noncollagenous components of the extracellular matrix (ECM), such as fibronectin and laminin [17–19]. In addition, plasmin is involved in proteolytic activation of additional proteases, for example, matrix metalloprotease (MMP) zymogens, including pro–MMP-1 and pro–MMP-3 [20,21].

Extensive evidence implicates elevated expression of uPA in malignant cells and the activity of uPA/plasmin in overall tumor progression and metastasis [7,9,22,23]. Inhibition of uPA activity by antibody and small molecule inhibitors has been shown to diminish tumor growth, angiogenesis, and metastasis in several model systems [6,10,24]. In addition, small interfering RNA and short hairpin RNA knockdown of uPA expression in prostate carcinoma cells diminished their invasion *in vitro* and tumor growth, angiogenesis, and dissemination to the lung in an orthotopic mouse model [25,26], and significantly reduced bone tumor burden and bone destruction in a bone metastasis xenograft model [27]. Furthermore, small interfering RNA targeting of the uPA promoter also decreased tumor growth, angiogenesis, and metastasis of prostate carcinoma cells [28]. However, because of the coordinate inhibitory effects on tumor growth, it was difficult to discriminate in these studies direct inhibitory effects of uPA RNA silencing on tumor metastasis from indirect consequences of reduced primary tumor size.

Some of the most compelling data implicating the plasminogen activation cascade in tumor progression come from transgenic mice deficient in various components of the PA system. Interestingly, most phenotypes associated with plasminogen deficiency were not observed in mice with an additional deficiency in fibrinogen [29]. However, in the MMTV-PymT model of breast carcinogenesis combined with genetic deficiency in plasminogen, spontaneous metastasis was significantly reduced without major effects on primary tumor growth [30]. Similarly, uPA deficiency resulted in greatly reduced levels of lung metastasis from MMTV-PymT–induced mammary carcinomas without affecting their growth [31]. Therefore, the single deficiency in uPA was sufficient to reduce metastasis, affirming that uPA is the major plasminogen activator functioning during tumor dissemination.

Despite all the evidence indicating that the uPA/plasmin system plays a critical role in tumor metastasis, the functional contributions of pro-uPA activation and uPA activity in the individual steps involved in the metastatic cascade remain to be elucidated. Using a chemical proteomic approach and function-blocking antibodies, our laboratory has previously identified activation of pro-uPA as a likely key step in the intravasation and metastatic spread of a highly disseminating variant of human HT-1080 fibrosarcoma [32,33]. We have recently isolated a pair of PC-3 prostate carcinoma cell variants with high and low dissemination capacities, namely, PC-hi/diss and PC-lo/diss, and showed that these cell variants exhibit a differential in uPA secretion and uPA activation [34].

In the present study, we sought to identify those individual events during metastatic progression that involve uPA activation. The function-blocking monoclonal antibody (mAb) 112 that uniquely prevents activation of the human pro-uPA zymogen has been used to address the contributory roles of tumor-produced uPA and uPA-generated plasmin in specific processes involved in cancer metastasis. Our findings from several quantitative *in vitro* and *in vivo* models demonstrate that uPA activation and plasmin activity are critically involved in early metastatic events, particularly in the invasive escape from the primary tumor, which we monitored in a newly developed *in vivo* model of tumor cell escape. Furthermore, toward defining the molecules mediating the effects of the uPA/plasmin activation cascade, we demonstrate that cleavage of matrix fibronectin by tumor uPA-generated plasmin results in enhanced migration-inducing capacity of the cleaved fibronectin. Together, our findings underscore a mechanism, by which elevated levels of uPA expression, activation, and activity render cancer cells with a high malignant potential due to enhanced invasive escape from primary tumors along the plasmin-modified ECM.

Materials and Methods

Tissue Culture

Dissemination variants derived from the human PC-3 prostate carcinoma cell line, PC-hi/diss and PC-lo/diss [34], were maintained in Dulbecco modified Eagle medium (DMEM) supplemented with 10% fetal calf serum and 10 µg/ml gentamicin (D10).

Antibodies

The following polyclonal and mAbs were used: anti–human pro-uPA mAb-112 [33], anti–human CD44 mAb 29-7 [34], anti–human β_1 integrin mAb P5D2 (R&D Systems, Minneapolis, MN) and α_5 integrin mAb P1D6 (Chemicon, Temecula, CA), rabbit anti-CD31 (Abcam, Cambridge, United Kingdom), and murine control IgG (Jackson ImmunoResearch, West Grove, PA). The supernatants from hybridomas B3/D6 (anti–avian fibronectin) and "31 or 31-2" (anti-avian laminin), developed by D.M. Fambrough, were obtained from the Developmental Studies Hybridoma Bank developed under the auspices of the National Institute of Child Health and Human Development and maintained by the Department of Biology at the University of Iowa (Iowa City, IA).

Orthotopic Prostate Tumor Model

Orthotopic implantations of PC-hi/diss cells into the prostates of immunodeficient mice were performed as described in Conn et al. [34]. Briefly, 8- to 9-week-old NOD-SCID mice were purchased from the TSRI breeding colony and maintained under the guidelines of the TSRI Institutional Animal Care and Use Committee. Mice were anesthetized with ketamine/xylazine and 2×10^6 of firefly luciferase–labeled PC-hi/diss cells in 30 µl of SF-DMEM were implanted into the anterior prostates through an incision in the lower abdomen. After 7 days, the mice were noninvasively imaged by IVIS (Caliper Life Sciences, Mountain View, CA) and separated into two treatment groups containing mice with tumors of similar sizes. Mice received intraperitoneal injections of 150 µg of mAb-112 or control IgG in 150 µl of phosphate-buffered saline (PBS) every 4 to 5 days. Mice were imaged again on day 27 and sacrificed at day 28. Exposed primary tumors were photographed, excised, and weighed, and internal organs were harvested and frozen for *Alu* quantitative polymerase chain reaction (qPCR) analysis. Three separate experiments, involving a total of 14 mice treated with control IgG and 11 mice treated with mAb-112, were performed.

Fold changes in levels of metastasis in both treatment groups were calculated compared with the mean of the IgG control group for each individual experiment, and the fold differences from independent experiments were combined.

Chick Embryo Model for Spontaneous Metastasis

The chick embryo spontaneous metastasis model was performed exactly as described [34]. Briefly, 2.0×10^6 PC-lo/diss or PC-hi/diss cells in 25 μl of SF-DMEM were grafted onto the chorioallantoic membrane (CAM) of 10-day-old embryos. For imaging experiments, PC-lo/diss and PC-hi/diss cells were prelabeled with 5 μM Cell-Tracker Green CMFDA (Molecular Probes, Invitrogen, Carlsbad, CA) according to the manufacturer's instructions. Developing PC-hi/diss tumors were treated on days 2 and 4 with 25 μg/embryo of mAb-112 or control IgG or 0.5 trypsin inhibitory units (TIU) of aprotinin in a 100-μl solution containing 5% DMSO. After 5 days, tumor-bearing embryos were injected with rhodamine-conjugated *Lens culinaris* agglutinin (LCA; Vector Labs, Burlingame, CA), and tumors were excised, stretched on glass slides, and imaged immediately using a Carl Zeiss AxioImager M1m microscope (Carl Zeiss Microimaging GmbH, Göttingen, Germany). Images were captured using AxioVision Re.4.6 software (Carl Zeiss Microimaging GmbH) and processed using Adobe Photoshop. Alternatively, for immunohistochemical analysis and quantitative analysis of tumor cell dissemination, embryos were sacrificed on days 6 and 7, respectively. Tumors were weighed, excised, and fixed in Zn-formalin or frozen in OCT, and portions of CAM distal to the primary tumor site were harvested and frozen for *Alu*-qPCR analysis to determine the numbers of spontaneously disseminated human tumor cells.

Chick Embryo Experimental Metastasis Model

Vascular arrest, extravasation, and colonization of PC-lo/diss and PC-hi/diss cells were analyzed in an experimental metastasis model, where 100 μl of 1×10^6 CellTracker Green–labeled cells per milliliter of SF-DMEM was injected directly into the allantoic vein of 12-day-old embryos. Where indicated, 0.1 TIU of aprotinin or 25 μg of mAb-112 or control IgG was injected per embryo along with the cells. After 10 minutes or 2 hours, groups of embryos were injected with rhodamine-conjugated LCA, and portions of the CAM were excised and immediately imaged without fixation using a Carl Zeiss AxioImager microscope as described above. The levels of CAM colonization were determined by *Alu*-qPCR analysis 5 days after tumor cell injections.

Quantitative Alu-PCR Analysis

Quantification of disseminated human tumor cells in chick or murine organs was performed essentially as described [35,36]. Briefly, genomic DNA was extracted from the tissue of interest using the Puregene DNA purification system (Qiagen, Minneapolis, MN). Real-time PCR was performed to amplify primate-specific *Alu* repeat sequences using 10 ng of extracted genomic DNA as a template in a Bio-Rad MyIQ LightCycler (Bio-Rad, Hercules, CA). The dsDNA binding dye SYBR green (Molecular Probes, Invitrogen) was used for quantification. The cycle threshold (C_t) values were converted into numbers of human cells using a standard curve generated by spiking constant numbers of chicken or murine cells with serially diluted human tumor cells.

Intramesodermal Microtumor Model for Tumor Escape and Early Invasion In Vivo

PC-lo/diss and PC-hi/diss cells were labeled with 5 μM CellTracker Green and resuspended at 2×10^6/ml. Small boluses of tumor cells

(3-5 μl) were injected directly into the mesoderm of day 9 chick embryos developing *ex ovo*. Each embryo received four to six individual injections. The developing PC-hi/diss microtumors were treated on day 2 with 25 μg of mAb-112, mAb P1D6, or control IgG; 0.125 TIU aprotinin; or 25 μl of 1 mM GM6001 (Calbiochem, EMD Chemicals Inc., Gibbstown, NJ). Where indicated, the embryos were treated with aprotinin on day 4 instead of day 2. On day 6 of microtumor development, embryos were injected intravenously with rhodamine-LCA; portions of the CAM with the microtumors were excised and immediately imaged using a Carl Zeiss AxioImager microscope. Quantification of tumor cell escape was performed using ImageJ software (public domain, NIH, Bethesda, MD). The mean of the five longest invasive distances from the microtumor-CAM border was determined for each microtumor, and at least 10 individual microtumors from three to five embryos were analyzed for each variable.

Three-dimensional Model for Tumor Cell Invasion In Vitro

PC-hi/diss cells were incorporated at a density of 1×10^6 cells/ml into neutralized type 1 rat tail collagen used at 2.2 mg/ml (BD Biosciences, Bedford, MA). Polymerized tumor cell–containing collagen droplets (25 μl each) were placed atop polymerized collagen gels (1.5 mg/ml) supplemented with EGF (20 ng/ml) and overlaid with additional 600 μl of the collagen/EGF mixture, providing a three-dimensional matrix for cell-containing droplets after final polymerization.

Fibrin-containing three-dimensional gels were prepared by mixing bovine fibrinogen (Sigma, Saint Louis, MO) with collagen to final concentrations of 3 and 1.5 mg/ml, respectively. Thrombin (Sigma) was added at a final concentration of 10 U/ml. For fibronectin-containing collagen gels, human fibronectin (BD Biosciences) was added to a final concentration of 20 μg/ml. Both fibrin- and fibronectin-enriched collagen gels were additionally supplemented with EGF to induce directional invasion of tumor cells from collagen droplets.

After final polymerization, three-dimensional gels with cell-containing collagen droplets were overlaid with 0.5 ml of AIM-V medium, containing 0.1% chicken serum (as a source of plasminogen) and 25 μg/ml control IgG or mAb-112. Culture medium supplemented with the corresponding antibodies was replaced every 3 to 4 days. On day 10, tumor cell spheroids were imaged with an Olympus CKX41 microscope equipped with an Infinity1 camera (Olympus America Inc., Center Valley, PA), and images were captured using Infinity Capture software. The distances invaded by the escaping tumor cells were measured using ImageJ software. At least six independent fields per variable were analyzed. The average length of invasion per field was multiplied by the number of invading cells/cell clusters per field to calculate the invasion index, and the average invasion index was determined for individual spheroids and presented as the mean for each treatment condition.

Immunohistochemistry

Normal CAM, primary PC-hi/diss CAM tumors and mouse prostate xenografts were excised and frozen in OCT for CD44, fibronectin, and laminin staining or fixed in Zn-formalin and paraffin-embedded for the Masson trichrome, fibrin, or CD31 staining. Frozen sections were fixed in 2% paraformaldehyde, blocked, and probed with 1 μg/ml of mAb-29-7 or hybridoma supernatants diluted 1:10. Standard Masson trichrome staining was performed by the Histology Core Facility at the Scripps Research Institute on paraffin-embedded tumor sections. For fibrin(ogen) staining, CAM tumor sections were probed with rabbit antifibrin (DAKO, Carpentia, CA) diluted 1:300, which cross-reacts

with avian fibrin. Mouse xenograft tumor sections were probed with 5 μg/ml rabbit anti-CD31.

After incubations with primary antibodies, sections were probed with corresponding biotinylated secondary antibodies (Vector Labs). All stained tissue sections were finally incubated with avidin-D horseradish peroxidase (HRP) conjugate (Vector Labs) for 30 minutes, developed with a diaminobenzidine chromogenic substrate, and counterstained with Mayer hematoxylin. Images were captured using an Olympus BX60 microscope equipped with a digital DVC videocamera (DVC, Austin, TX) and processed with Adobe Photoshop 6.0 software.

Western Blot Analysis

Conditioned medium (CM) from equal cell numbers (as determined by cell counting) or cell lysates containing equal amounts of proteins (as determined using the BCA protein assay; Pierce; Thermo Scientific, Rockford, IL) were boiled in SDS buffer with or without 100 mM dithiothreitol. Samples were separated on 4% to 20% Trisglycine SDS-PAGE gels (Invitrogen) and transferred to Immobilon-P polyvinylidene fluoride membranes (Millipore, Billerica, MA). Membranes were blocked in PBS–Tween 20 containing 5% milk and probed with the indicated primary antibodies. Membranes were incubated with secondary anti-rabbit (Pierce) or antimouse (Bio-Rad) HRP-conjugated antibodies, and immunoreactive bands were visualized using SuperSignal West Pico Chemiluminescent Substrate (Pierce).

uPA Activation

PC-lo/diss and PC-hi/diss cells were seeded at equal densities and incubated overnight in D10. Cell monolayers were washed briefly with serum-free DMEM (SF-DMEM), which seems to preserve traces of serum plasminogen associated with the cell surfaces. Cell monolayers were then overlaid with SF-DMEM for additional incubation for 24 or 48 hours. Where indicated, the cells were incubated in the presence of 0.1% chicken serum, as a source of additional plasminogen, and 25 μg/ml control IgG or mAb-112, 0.1 TIU/ml aprotinin, or 20 μg/ml α_2-antiplasmin (Calbiochem). The activation status of uPA in the CM was analyzed by Western blot analysis under reducing conditions.

Plasmin Generation Assays and uPA Activity Measurements

For plasmin generation, CM was incubated at 37°C with 10 μg/ml human plasminogen (123 nM) and 0.5 mM S-2251 chromogenic plasmin substrate (Chromogenix Instrumentation Laboratory, Lexington, MA). Where indicated, the CM was preincubated with the chemical uPA inhibitor amiloride (50 μM), 167 nM (25 μg/ml) of mAb-112, or 4 μM aprotinin (0.1 TIU/ml) for 25 minutes at room temperature before the addition of plasminogen and S-2251. The OD was read at 405 nm every 1 minute or 2 minutes using a spectrophotometer. Background readings of CM and S-2251 in the absence of plasminogen were subtracted.

To measure uPA-generated plasmin activity at the cell surface, cell monolayers were extensively washed and then incubated for 15 minutes with 8 μg/ml of plasminogen (100 nM). The collected supernatants were incubated with 0.5 mM of S-2251 substrate to determine plasmin activity. Alternatively, after an extensive wash, cell monolayers were treated with pH 3.5 glycine-HCl containing isotonic NaCl for 10 minutes at room temperature to strip cell surface–bound uPA. The solution was neutralized with 50 mM HEPES, and the plasmin-generating capacity of the stripped uPA was analyzed as described previously using S-2251 and human plasminogen.

Fibronectin Cleavage and Tumor Cell Migration in Transwells

Human fibronectin (200 μg/ml) was incubated overnight at 37°C with human plasmin (Sigma) at a 10:1 molar substrate/enzyme ratio in the presence or absence of 1 TIU/ml aprotinin. Alternatively, fibronectin was incubated overnight at 37°C in PC-hi/diss CM alone or in the presence of 12 μg/ml human plasminogen with or without 1 TIU/ml aprotinin. Samples containing 5 μg of fibronectin were separated by SDS-PAGE on 4% to 20% Tris-glycine gels under nonreducing conditions. The gels were stained with Coomassie blue dye to visualize the major protein bands.

For fibronectin-induced migration, the undersides of Transwell membranes with 8-μm pores (Corning Life Sciences, Pittston, PA) were coated with 10 μg/ml fibronectin for 1 hour at 37°C. To partially cleave the coated fibronectin, the Transwells were incubated overnight at 37°C with plasmin (5 μM). PC-hi/diss cells were placed at 1×10^5 per insert in SF-AIM-V medium and allowed to migrate for 18 to 24 hours. Cells in the outer chambers were collected and counted. Experiments were performed in duplicate, with two wells per variable in each experiment.

Data Analysis and Statistics

Data processing and statistical analysis were performed using GraphPad Prism (GraphPad Software, Inc, San Diego, CA). Data were considered significantly different for $P < .05$ in Student's t test or Mann-Whitney U test.

Results

High Levels of Pro-uPA Activation and uPA-Generated Plasmin Activity Correspond to High Levels of Tumor Cell Dissemination

To assess whether the respectively high- and low-dissemination capacities of the PC-hi/diss and PC-lo/diss cell variants correlated with their ability to generate active plasmin, a coupled plasmin activity assay was performed on samples of CM. In this assay, exogenous plasminogen must be activated to cleave the plasmin-specific substrate, S-2251. Substantially enhanced plasmin generation was observed in PC-hi/diss CM compared with PC-lo/diss CM (Figure 1A, *graphs*), consistent with higher levels of total uPA protein, represented by the single-chain pro-uPA and also the two-chain active uPA, which accumulated in the PC-hi/diss CM during 24 hours of incubation, as judged by Western blot analysis (Figure 1A, *right*).

Because cell surface protease localization facilitates the efficient proteolysis of ECM and transmembrane molecules, we also examined the ability of PC-hi/diss and PC-lo/diss cells to generate active plasmin at the cell surface. Purified plasminogen was incubated for 15 minutes directly with cell monolayers of increasing densities of PC-lo/diss or PC-hi/diss cells, and the extent of plasmin generation was determined by measuring S-2251 cleavage in the resulting supernatants (Figure 1B). In this approach, most of the generated plasmin results from the activity of cell surface uPA because the short incubation time does not yield significant levels of secreted uPA. In a second confirmatory approach, cell surface–bound uPA was stripped from PC-lo/diss and PC-hi/diss culture monolayers, and the ability of the released uPA to activate plasminogen was assessed using the chromogenic assay (Figure 1C). Both methods indicated substantially greater cell surface plasmin-generating capacity associated with the PC-hi/diss cells compared with the PC-lo/diss cells. It is important to note that the differential in cell surface uPA activity between the PC-3 variants was not attributable to differences in the expression of uPA receptor uPAR because uPAR levels were similar

between the low- and high-disseminating counterparts (Figure W1). Thus, the PC-3 variants not only manifest differential secreted and surface levels of pro-uPA and active uPA protein but also exhibit a substantial differential in functional plasmin-generating capacities, both at the cell surface and in the solution.

The detection of active uPA in the CM and on the surface of PC-hi/diss cells indicated the presence of a pro-uPA activator in the model systems. Although the transmembrane serine proteases matriptase and hepsin have been demonstrated to activate uPA [37–39], the gene expression levels of both these proteases in the PC-hi/diss cells were extremely low or undetectable (data not shown). However, plasmin generated from plasminogen is known to be a major feedback activator of

pro-uPA [8], and both plasma and serum are the major natural sources of plasminogen *in vivo* and *in vitro*. When the PC-hi/diss cells were supplemented with 0.1% chicken serum as a source of plasminogen/plasmin, nearly all secreted pro-uPA (>95%) was activated to the two-chain form, suggesting that serum plasmin could be a major pro-uPA activator (Figure 1*D*, *lane 1*). To confirm this notion, the potent plasmin inhibitor, aprotinin, and the natural plasmin inhibitor, α₂-antiplasmin, were added to the PC-hi/diss cell cultures. Both inhibitors completely abrogated the conversion of PC-hi/diss pro-uPA to the two-chain active uPA, strongly implicating serum plasmin as a major feedback activator of pro-uPA in this system (Figure 1*D*, *lanes 2 and 4*). In addition, generation of the two-chain uPA was almost completely inhibited by
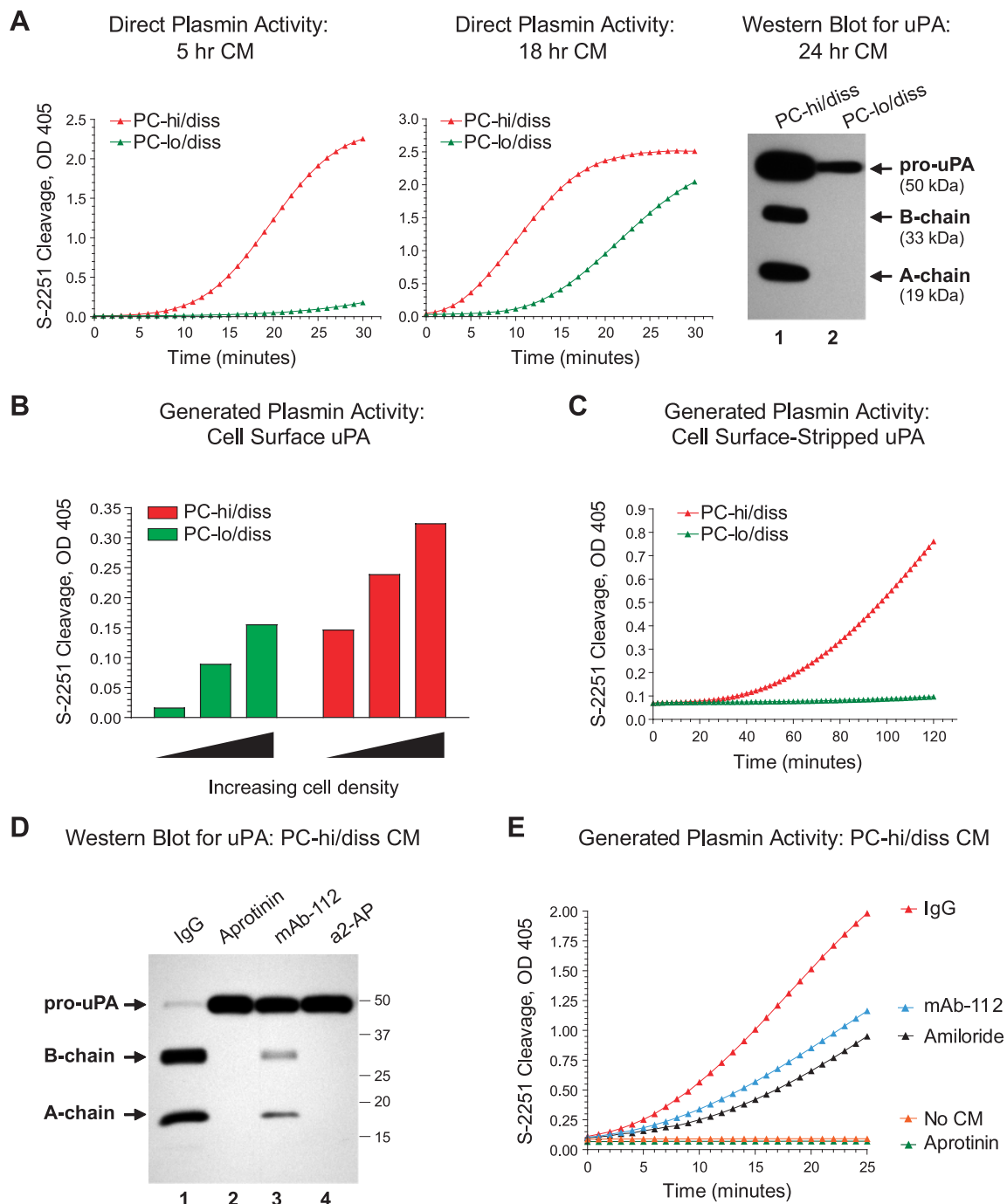
anti-uPA mAb-112 (Figure 1D, lane 3), previously shown to specifically block activation of pro-uPA [33]. Therefore, plasmin-mediated activation of pro-uPA can be effectively prevented in vitro by specifically blocking either plasmin activity or pro-uPA activation.

Furthermore, when mAb-112 was incorporated into the PC-hi/diss CM, the rate of S-2251 cleavage in a plasmin generation assay was significantly reduced, further implicating pro-uPA activation in a feedback uPA/plasmin(ogen) activation cascade (Figure 1E). The uPA activity-blocking inhibitor, amiloride, also substantially slowed the plasmin-generating ability of PC-hi/diss CM. As expected, the direct targeting of plasmin with aprotinin completely inhibited the uPA-generated plasmin activity (Figure 1E). These in vitro findings suggested that specific inhibition of pro-uPA activation with mAb-112 might produce substantial inhibitory effects on plasmin generation in metastasis assays in vivo.

Inhibition of Pro-uPA Activation Reduces Invasion and Spontaneous Dissemination of PC-hi/diss Cells in an Orthotopic Xenograft Model

To determine the functional contribution of uPA activation to carcinoma cell dissemination, we used mAb-112 in an orthotopic xenograft model, in which PC-hi/diss cells were implanted into the prostates of NOD/SCID mice. Seven days after cell implantations, tumor-bearing mice were imaged and separated into two groups for treatment with mAb-112 or control mouse IgG, delivered intraperitoneally every 4 days (Figure 2A, top). On day 28, large primary tumors that had developed within the prostate region were observed in both groups of mice (Figure 2A, bottom). The presence of large prostate primary xenografts of similar size was visually confirmed in both treatment groups (Figure 2B, left). The weights of the primary PC-hi/diss prostate tumors indicated no significant differential in tumor growth between the control IgG- and mAb-112–treated mice (Figure 2D).

The axial and subiliac lymph nodes (LNs) were enlarged in both treatment groups, although node enlargement was more pronounced in the control mice (Figure 2B, middle). A similar trend was noted for the rate of mesenterium colonization, observed in 45% of control mice versus 25% of mAb-112–treated animals. Furthermore, control animals developed much larger tumor colonies on the mesenterium compared with mAb-112–treated mice (Figure 2B, right), indicating inhibitory effects of mAb-112 on intraperitoneal dissemination of PC-hi/diss tumor cells.

To analyze the effects of mAb-112 treatment on tumor development and local invasion, adjacent sections of primary prostate tumors were immunostained with human-specific anti-CD44 antibody to highlight the human tumor cells and with anti-CD31 to highlight the murine blood vessels (Figure 2C). Whereas the tumors from control IgG-treated mice manifested jagged invasive fronts and nests of escaped tumor cells (Figure 2C, two left panels in IgG control), the tumors from mAb-112–treated mice appeared confined and exhibited smooth tumor borders (Figure 2C, top panels in mAb-112 group). Furthermore, whereas PC-hi/diss primary tumor cells from the control mice were observed in close association with CD31-positive blood vessels and detected intravascularly (Figure 2C, right panels in IgG control), the tumor cells from mAb-112–treated mice did not seem to engage in such interactions, even in areas with relatively high vessel density (Figure 2C, right panels in mAb-112 group). Thus, the immunohistochemical analysis of the orthotopic prostate xenografts indicated that treatment with mAb-112 reduced local invasion and tumor cell–blood vessel interactions.

Levels of tumor cell dissemination to internal organs were quantified by Alu-qPCR, which indicated that, compared with the control, the mAb-112 treatment significantly diminished PC-hi/diss metastasis to the lungs (by 58%, $P < .05$), liver (by 67%, $P < .05$), and brain (by 87%, $P < .01$). Levels of metastasis in the colonized LNs were also decreased by 50% in the inguinal LNs and by 54% in the axillary LNs; however, although a clear trend was observed, the diminishment was not statistically significant (Figure 2D). Overall, the findings from the orthotopic implantation model indicated that blocking activation of tumor cell–produced pro-uPA can significantly inhibit levels of spontaneous dissemination by highly malignant prostate carcinoma cells.

Figure 1. High levels of plasmin-generating ability of PC-hi/diss cells correlate with high levels of secreted and cell surface uPA and its activation status. (A) Plasmin-generating activity of uPA secreted by PC-hi/diss and PC-lo/diss cells. CM from PC-hi/diss and PC-lo/diss cultures was collected after 5 (left graph) and 18 hours (right graph) of incubation. Plasminogen was added to the CM to a final concentration of 123 nM, and cleavage of chromogenic plasmin substrate, S-2251, was analyzed at indicated time points by measuring optical density at 405 nm. Far right: uPA detected by Western blot analysis under reducing conditions in 24 hr CM from PC-lo/diss and PC-hi/diss cells (lanes 1 and 2, respectively). Positions of the 50-kDa proenzyme, 33-kDa B-chain, and 19-kDa A-chain are indicated by arrows. (B) Plasmin-generating activity of cell surface–associated uPA. PC-hi/diss and PC-lo/diss cells were seeded at increasing densities, washed and incubated for 15 minutes in SF-DMEM supplemented with 100 nM plasminogen, followed by direct measurement of plasmin activity with the chromogenic substrate, S-2251. (C) Plasmin-generating activity of receptor-bound uPA. Cell surface uPA was stripped from the PC-lo/diss or PC-hi/diss cell monolayers with a 10-minute isotonic acid wash. After neutralization, plasmin-generating ability of stripped uPA was determined in a coupled S-2251 cleavage assay in the presence of 123 nM plasminogen. (D) Activation status of uPA produced by PC-hi/diss cells and its inhibition by serine protease inhibitors and activation-blocking mAb-112. PC-hi/diss cells were incubated with control IgG, anti-uPA mAb-112, or indicated inhibitors, aprotinin and α$_2$-antiplasmin (a2-AP). Chicken serum was added at 0.1% to the cultured cells as a source of plasminogen to initiate a plasmin-generating cascade. After incubating for 48 hours, samples of CM were analyzed by Western blot for uPA. Lane 1, pro-uPA is almost completely converted to a two-chain enzyme in the IgG control; lanes 2 and 4, aprotinin and a2-AP completely abrogated activation of pro-uPA; lane 3, mAb-112 significantly inhibited conversion of single-chain pro-uPA zymogen into the two-chain uPA enzyme. Positions of the molecular weight markers (kDa) are indicated on the right. (E) Inhibition of uPA-generated plasmin activity by mAb-112. CM, containing a mixture of pro-uPA and active uPA produced by PC-hi/diss cells cultured in SF-DMEM for 24 hours, was incubated with control IgG, mAb-112, the chemical inhibitor of uPA activity amiloride or the plasmin inhibitor aprotinin. Plasminogen and the chromogenic S-2251 substrate were added to the CM to final concentrations of 100 and 0.5 mM, respectively, and the activity of the generated plasmin was determined by rate of S-2251 cleavage. Aprotinin completely prevented S-2251 cleavage, and there was no S-2251 cleavage in the presence of plasminogen alone (No CM).

Preventing uPA Activation Reduces Capacity of Tumor Cells to Complete Early Metastatic Events in the Chick Embryo CAM Model

The inhibitory effects of mAb-112 on PC-hi/diss on overall spontaneous dissemination (Figure 2) could be caused by blocking pro-uPA activation either during early metastatic events (i.e., those leading to intravasation) or during later events (such as survival in circulation, arrest, and colonization). To address the functional contribution of uPA activation to various steps in the metastatic process, we turned to chick embryo models, which allow for efficient and quantitative analysis of tumor cell intravasation as well as for direct imaging of tumor cells during specific stages of the metastatic process.

Because mAb-112 reduced local invasion in the prostate xenograft model, we first analyzed whether a similar effect would be elicited in pri-mary CAM tumors. To this end, PC-hi/diss cells were labeled with Cell-Tracker dye and grafted atop the CAMs of day 10 chick embryos. The developing tumors were left untreated or treated topically with mAb-112, to inhibit pro-uPA activation, or aprotinin, to inhibit plasmin activity. In parallel, PC-lo/diss cells, expressing low levels of pro-uPA, were also pre-labeled with CellTracker and then grafted onto the CAM. After 5 days, the embryos were injected with rhodamine-conjugated LCA to highlight the avian vasculature, and primary tumors were immediately analyzed using a fluorescence microscope. Whereas primary tumors developed from PC-lo/diss cells displayed smooth borders and almost complete absence of invasion, PC-hi/diss tumors manifested jagged borders and extensive collective invasion of tumor cells into the surrounding CAM tissue (Figure 3A). However, the treatment of developing PC-hi/diss tumors with mAb-112 or aprotinin substantially reduced the extent of
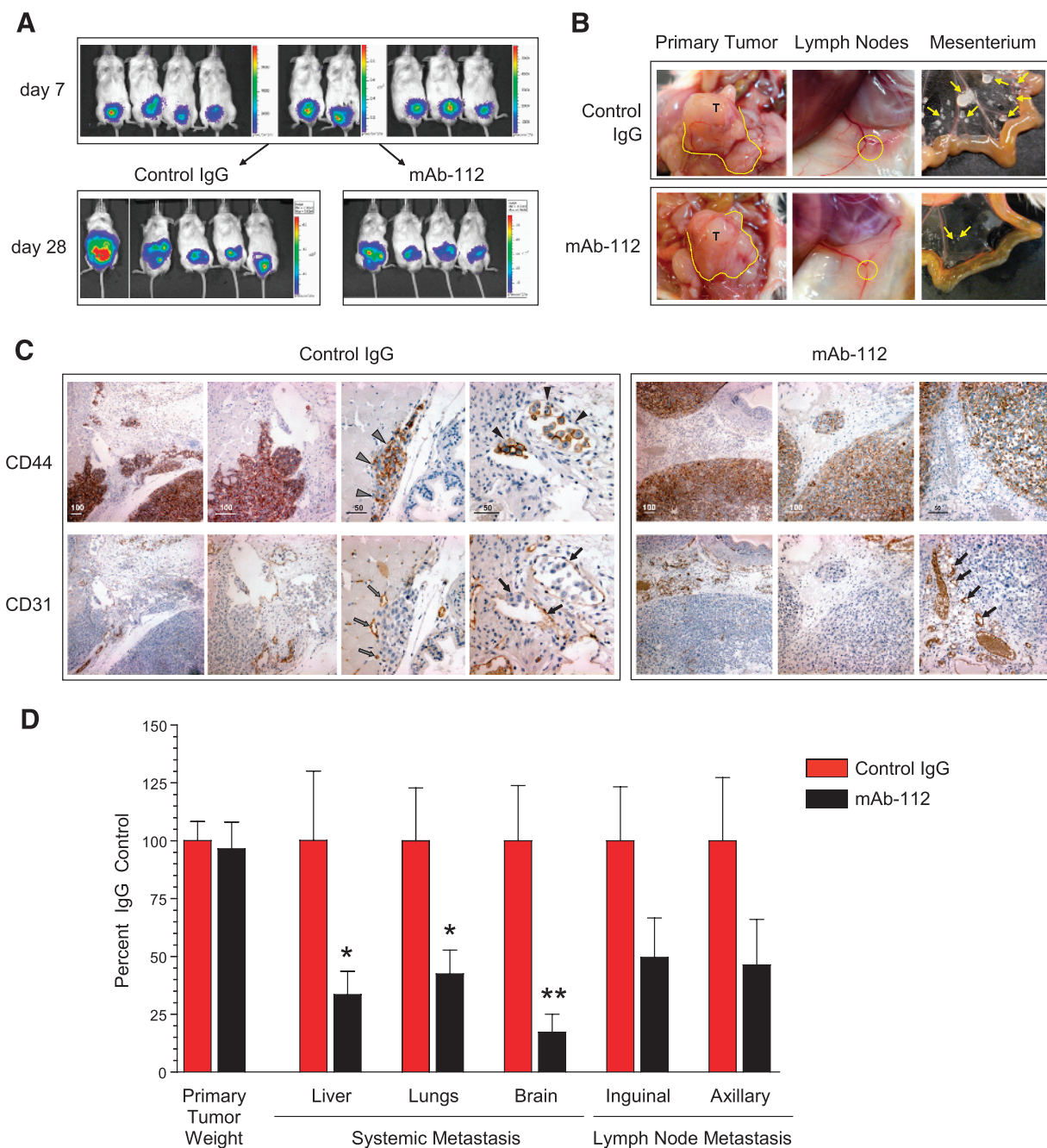
primary tumor invasion (Figure 3A), implicating pro-uPA activation and active uPA-generated plasmin, respectively, in the invasive processes at the primary tumor site. Quantification of actual numbers of disseminated tumor cells in the distal CAM by *Alu*-qPCR confirmed that both mAb-112 and aprotinin dramatically reduced spontaneous dissemination from PC-hi/diss tumors almost to the levels of the nondisseminating PC-lo/diss variant (Figure 3B). These profound inhibitory effects of blocking the uPA/plasmin system on local invasion and spontaneous metastasis of PC-hi/diss cells indicated that pro-uPA activation and uPA-generated plasmin activity can play critical roles during early metastatic events.

To address potential effects of mAb-112 and aprotinin on later metastatic events, especially vascular arrest and initial extravasation, PC-hi/diss cells were labeled with CellTracker and directly injected into the CAM vasculature in the presence or absence of aprotinin or mAb-112, thereby bypassing the intravasation step. In parallel, CellTracker Green–prelabeled PC-lo/diss cells were also inoculated into the chick embryo vasculature. After 10 minutes, both PC-lo/diss and PC-hi/diss cells seemed to be in circulation because most of the injected tumor cells in the CAM were observed intravascularly (Figure 4A, *top*). However, by 2 hours, the PC-lo/diss and PC-hi/diss cells had already arrested in the terminal capillaries and had begun to extravasate from the capillary plexus. PC-hi/diss cells seemed similarly capable of efficient arrest and extravasation at 2 hours in the embryos injected with control IgG, mAb-112, or aprotinin (Figure 4A, *bottom*), suggesting that tumor cell arrest and exit from the vasculature can proceed in the absence of uPA activation and plasmin activity. Levels of CAM colonization by PC-lo/diss and PC-hi/diss cells were quantified 5 days after tumor cell injection by *Alu*-qPCR. In contrast to the profound differential in spontaneous dissemination from primary PC-lo/diss and PC-hi/diss tumors, the levels of colonization were similar between PC-lo/diss and PC-hi/diss variants (Figure 4B). The levels of CAM colonization by PC-hi/diss cells were not significantly reduced by mAb-112 (23% of control, $P = .142$) but were diminished 44% by aprotinin (Figure 4B), in sharp contrast to the dramatic inhibition of PC-hi/diss spontaneous metastasis by both mAb-112 and aprotinin (Figure 3B). These results indicate that,

in our model systems, activated tumor cell–derived uPA may facilitate mainly early metastatic events such as primary tumor escape and invasive entry into the vasculature; however, the uPA/plasmin cascade may also have some effect on later metastatic events.

Functional Role of Pro-uPA Activation and uPA-Generated Plasmin Activity in Cell Escape from the Primary Tumor

To directly manipulate and quantify the extent of tumor invasion and tumor cell escape *in vivo*, we developed a model in which microtumors are established within the mesoderm layer of the CAM (Figure 5A). Within 5 to 6 days after microinjections, tumor cells can be observed escaping from well-formed microtumors and invading the surrounding stroma, making this model useful for testing the invasion-blocking activity of antiproteolytic agents.

Small boluses of CellTracker Green–labeled PC-lo/diss and PC-hi/diss cells were injected directly into the CAM mesoderm of day 9 embryos developing *ex ovo*. The developing PC-hi/diss microtumors were additionally treated with mAb-112, aprotinin or vehicle control. After six additional days, the embryos were injected with rhodamine-conjugated LCA, and the intramesodermal microtumors were imaged without fixation. In comparison with PC-lo/hiss, PC-hi/diss cells exhibited higher levels of tumor cell escape from intramesodermal microtumors (Figure 5, *B* and *C*). However, when PC-hi/diss microtumors were treated with mAb-112 or aprotinin on day 2 after cell injection, a significant and substantial reduction in invasion was observed compared to the control (Figure 5, *C-E*), which was confirmed by quantitative analysis (Figure 5H). Interestingly, a broad-spectrum MMP inhibitor, GM6001, did not have a significant effect on PC-hi/diss invasion (Figure 5, *G* and *H*), suggesting that MMP activity does not play a dominant role in the early escape of PC-hi/diss cells in this *in vivo* model system. Importantly, no significant inhibition of invasion was observed if PC-hi/diss microtumors were treated with aprotinin at a late time point, that is, on day 4 instead of day 2 (Figure 5, *F* and *H*), indicating that uPA-generated plasmin is functionally involved during initial tumor cell escape and invasion.

Figure 2. Inhibition of spontaneous metastasis of PC-hi/diss carcinoma cells in a murine orthotopic model of prostate cancer by treatment with mAb-112. (A) PC-hi/diss cells, tagged with firefly luciferase, were implanted into anterior prostates of NOD-SCID mice. After 7 days, mice were injected intraperitoneally with luciferin, imaged by IVIS and allocated evenly into two treatment groups. Levels of bioluminescence in the prostate region were similar at this time, indicating comparable initial tumor sizes (top panels). After 28 days, tumor-bearing mice treated with control IgG or mAb-112 were imaged again (bottom panels). One of the control mice presented extensive tumor cell ascites (far left bottom panel). However, levels of bioluminescence in the prostate area were similar in the mice from both treatment groups. (B) Gross morphology of primary prostate tumors (T, outlined with dotted line), enlarged inguinal LNs (circled with dotted line), and macroscopic tumor colonies in the mesenterium (yellow arrows). (C) Immunohistochemical staining of consecutive sections of prostate xenografts from mice treated with control IgG or mAb-112 (boxed panels on the left and right, respectively). To discriminate human tumor cells from the mouse stroma, sections were stained (brown) with human-specific anti-CD44 (top panels). Vasculature was highlighted (brown) by staining with anti-CD31 (bottom panels). In the control IgG group, gray arrowheads point to a nest of CD44-positive tumor cells (top), whereas gray arrows in a consecutive section point to the blood vessels associated with tumor nests (bottom). CD44-positive tumor cells, which seem to localize intravascularly, are indicated by black arrowheads (right top panel); the intravascular localization of these cells is confirmed by CD31 staining of capillaries indicated by solid black arrows (right bottom panel). In the mAb-112–treated group, black arrows (right bottom panel) point to blood vessels localized close to the tumor border, but not interacting with or encompassing the nearby tumor cells (brown staining, right top panel). Numbers above scale bars indicate length in micrometers. (D) Primary tumors were excised and weighed, indicating no difference in primary tumor size. Levels of metastasis to the liver, lungs, brain, and LNs (inguinal and axillary) were quantified by *Alu*-qPCR. Percent inhibition was calculated from pooled data for mAb-112–treated mice ($n = 11$) in comparison to IgG control mice ($n = 14$) in three individual experiments. Levels of metastasis in LNs were determined for the nodes positive for human cells; 9 of 14 inguinal and 11 of 14 axillary nodes were positive in the control group, whereas 7 of 11 nodes of both types were positive in the mAb-112 group. Bars represent means ± SEM. *$P < .05$, Mann-Whitney test. **$P < .05$, two-tailed Student's *t* test.
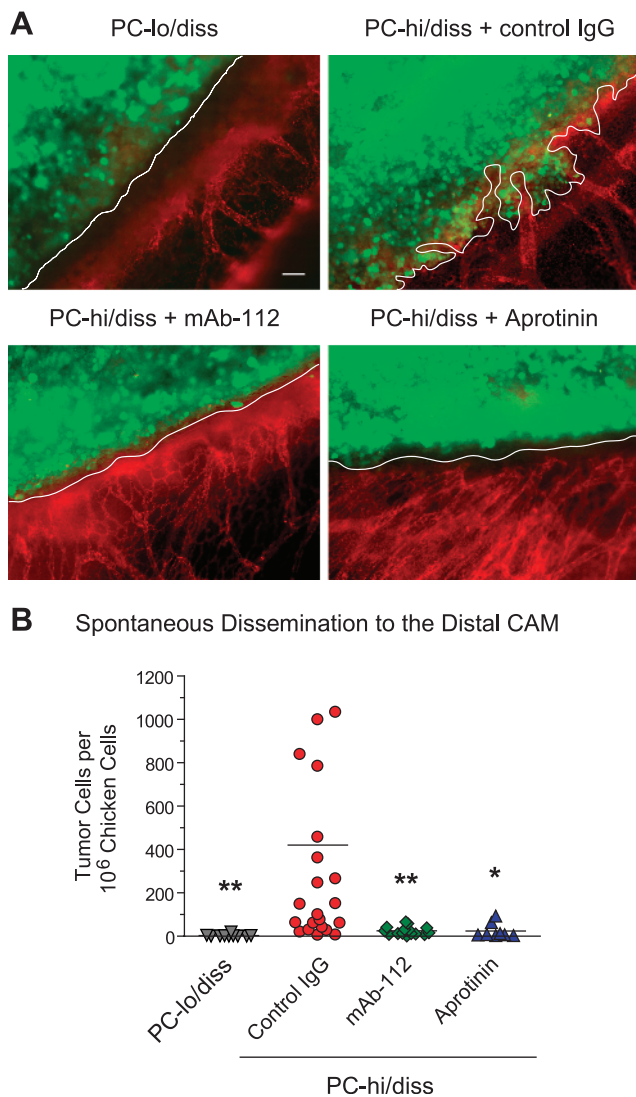
Figure 3. Tumor invasion in spontaneous metastasis is inhibited by interfering with uPA activation or plasmin activity. (A) Levels of local invasion in primary tumors. PC-lo/diss and PC-hi/diss cells were labeled with CellTracker Green and grafted onto the CAM. Developing PC-hi/diss tumors were additionally treated with control IgG, pro-uPA activation-blocking mAb-112, or the plasmin inhibitor aprotinin on days 2 and 4. On day 5, embryos were injected with rhodamine-conjugated lectin to highlight the CAM vasculature (red), and primary tumors (green) were immediately imaged without prior fixation. Tumor-CAM borders are indicated with white lines, illustrating significant CAM invasion only in the PC-hi/diss control tumors. Images were acquired at an original magnification of ×100. Scale bar, 50 μm. (B) Levels of spontaneous dissemination to the distal CAM were quantified after 7 days of tumor development by *Alu*-qPCR analysis. Data are presented as number of human cells per 10^6 chicken cells. A total of 8 to 21 embryos per variable were used in two independent experiments. Lines in scatter plots represent means. **$P < .01$ and *$P < .05$, two-tailed Student's *t* test.

Fibronectin as a Putative Substrate Mediating the Metastasis-Promoting Effects of uPA and uPA-Generated Plasmin

Although uPA itself has a very limited substrate specificity, uPA-generated plasmin has a broad substrate repertoire that includes

various noncollagenous matrix components. To determine whether canonical plasmin substrates might be deposited within the primary tumors or at the tumor borders, PC-hi/diss CAM tumors were immunohistochemically stained for the plasmin substrates fibronectin, laminin, and fibrin (Figures 6 and W2). The tumor distribution of collagen was also analyzed because plasmin is known to activate potent collagenases, such as MMP-1 and MMP-13, capable of efficient collagen cleavage [40,41]. A group of PC-hi/diss tumors treated with aprotinin were included in parallel staining to determine whether the diminishment of tumor invasion and metastasis caused by inhibiting the uPA/plasmin cascade would be accompanied by changes in the composition of the tumor tissue matrix.

PC-hi/diss primary tumors were stained with anti-human CD44 mAb to discriminate tumor cells within the CAM tissue (Figure 6, *top*). In consecutive sections, avian fibronectin was detected at high levels both at the tumor border and within tumors and seemed to accumulate especially in primary tumors treated with aprotinin (Figure 6, *middle*). Laminin, however, was not observed around or within primary tumors and was localized mostly to medium-to-large vessels in both treated and control tumors (Figure W2, *top*). Although fibrin is a critical physiological substrate of plasmin, only a few sparse intravascular fibrin deposits were detected in control and aprotinin-treated tumors (Figure W2, *bottom*). Extensive deposition of collagen compared to normal CAM was observed near the primary tumor border, but the pattern of collagen staining was not significantly affected by aprotinin treatment (Figure 5, *bottom*).

The immunohistochemical and histologic analyses of ECM components indicated that fibronectin and collagen were major components of the PC-hi/diss tumor stroma. To validate the involvement of active uPA in the invasion of PC-hi/diss cells into this complex tissue matrix, we used an *in vitro* model of three-dimensional tumor cell escape from spheroids into collagen gels enriched in specific ECM components and additionally supplemented with EGF to induce cell migration (Figure 7). If the matrix contained collagen alone, the presence of mAb-112 did not affect escape of PC-hi/diss cells from spheroids (Figure 7, *A* and *B*). However, when the canonical plasmin substrate, fibrin, was incorporated into the surrounding collagen matrix, cell escape was significantly inhibited by mAb-112 to 40% of control levels (Figure 7B). Furthermore, when fibronectin was added to the collagen scaffold, mAb-112 also reduced the PC-hi/diss tumor cell escape by 50% (Figure 7B). Thus, the *in vitro* escape of PC-hi/diss cells into both types of complex matrices requires uPA activation. These data are consistent with our *in vivo* results demonstrating that PC-hi/diss cells can escape from both primary CAM tumors and intramesodermal microtumors and that this escape into the more natural collagen/fibronectin–rich tumor stroma was sensitive to mAb-112.

Limited Cleavage of Fibronectin by uPA-Generated Plasmin Enhances PC-hi/diss Migration *In Vitro and May Contribute to $\alpha_5\beta_1$ Integrin-Mediated Tumor Escape In Vivo*

Cleavage of fibronectin can constitute one of the mechanisms whereby uPA-generated plasmin may contribute to increased cancer cell invasion and dissemination. Supporting this idea, Western blot analysis revealed a prominent increase in the levels of high-molecular weight fibronectin in the aprotinin-treated CAM tumors compared with control tumors (Figure W3), confirming the apparent accumulation of immunodetectable fibronectin in CAM tumors treated with aprotinin (Figure 6). We therefore further analyzed whether PC-hi/diss–mediated plasmin
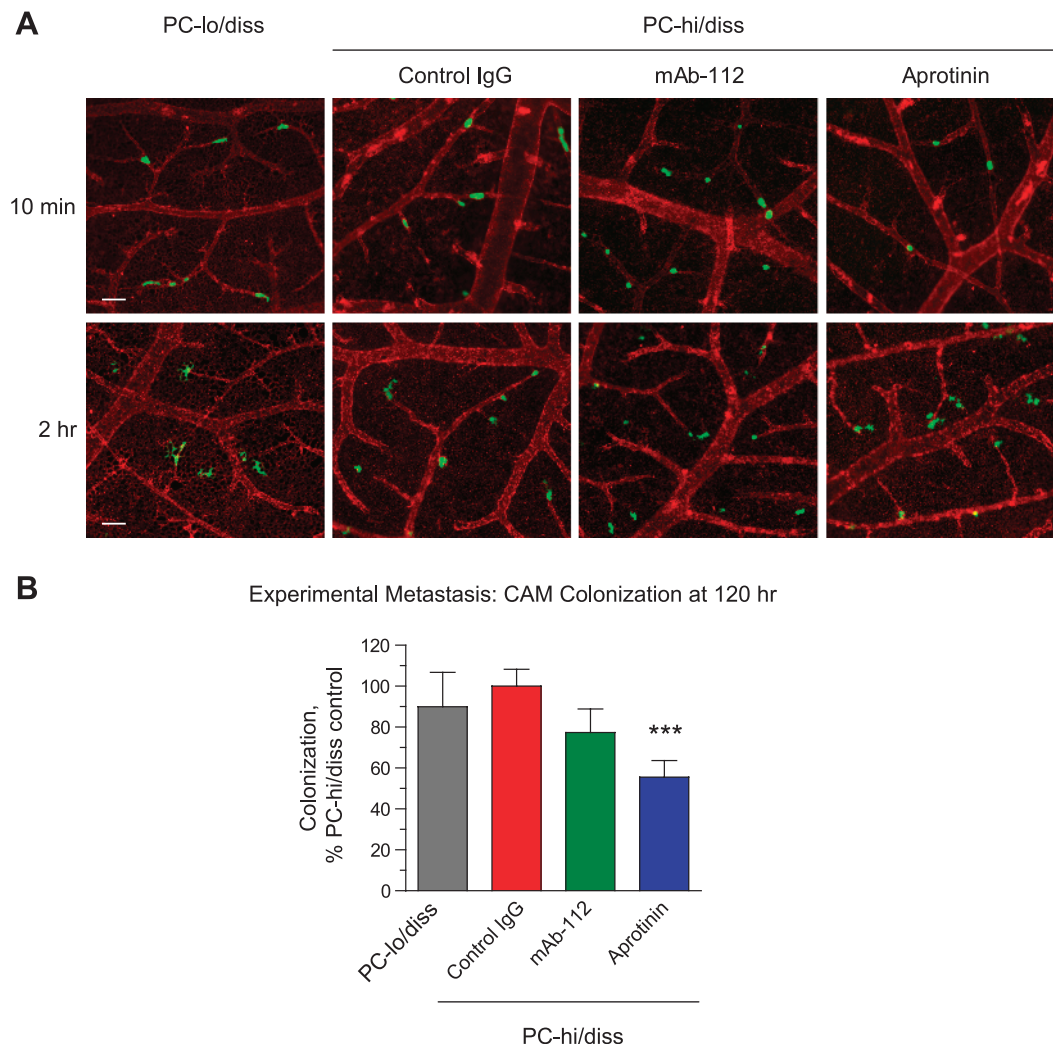
Figure 4. Initial stages of experimental metastasis is independent of uPA/plasmin(ogen) activation system. (A) Arrest and initial extravasation of tumor cells is independent of mAb-112 and aprotinin. Day 12 embryos were injected with rhodamine-conjugated lectin. After 15 to 20 minutes, single-cell suspensions of CellTracker Green–labeled PC-lo/diss cells or PC-hi/diss cells, mixed with control IgG, mAb-112, or aprotinin, were directly injected into the allantoic vein. Ten minutes and 2 hours later, portions of the CAM were immediately imaged by immunofluorescence microscopy. Green fluorescent tumor cells were visualized still within the CAM vasculature at 10 minutes (top) or as initiating extravasation from the ectoderm capillary plexus at 2 hours after injection (bottom). No major morphologic differences were observed between PC-lo/diss and PC-hi/diss cells or between the control IgG- and mAb-112– or aprotinin-treated PC-hi/diss cells. Images were acquired at an original magnification of ×100. Scale bar, 50 μm. (B) Levels of CAM colonization were determined by Alu-qPCR 5 days after intravenous inoculation of PC-lo/diss or PC-hi/diss cells mixed with indicated additives. Pooled data are presented from two (PC-lo/diss) to six (PC-hi/diss, aprotinin) individual experiments, using a total of 14 to 76 embryos per variant. Levels of colonization in individual embryos were determined as percent of PC-hi/diss control. Data are presented as mean ± SEM. ***$P < .001$.

generation would promote fibronectin cleavage and whether plasmin-cleaved fibronectin would induce PC-hi/diss cell migration.

First, fibronectin was incubated with PC-hi/diss CM in the presence or absence of plasminogen and aprotinin (Figure 8A). Although incubation of fibronectin in buffer (Figure 8A, $lane\ 2$) or with PC-hi/diss CM alone (data not shown) did not induce its cleavage, the addition of plasminogen to PC-hi/diss CM resulted in substantial cleavage of fibronectin into fragments of various sizes (Figure 8A, $lane\ 3$). This fragmentation of fibronectin was completely abrogated by aprotinin (Figure 8A, $lane\ 4$). Fibronectin was not cleaved when incubated with plasminogen in the absence of any source of active uPA (Figure 8, $lane\ 5$). Thus, these results indicate that the activation of plasmin by PC-hi/diss–derived plasminogen activators can drive the generation of functionally important fibronectin fragments.

We addressed whether plasmin-induced fibronectin fragmentation can functionally contribute to increased PC-hi/diss cell motility (Figure 8B). To this end, Transwells were coated with fibronectin and either left intact or incubated with plasmin in the presence or absence of aprotinin. Analysis of protein-stained gels confirmed partial, aprotinin-sensitive cleavage of fibronectin by plasmin (Figure 8B, $bottom$). The haptotactic migration of PC-hi/diss cells toward nontreated or plasmin-treated fibronectin indicated that limited cleavage of fibronectin by plasmin significantly enhanced PC-hi/diss migration by more than 2.5-fold and that this enhancement was sensitive to aprotinin (Figure 8B, $bar\ graph$). This cell migration response did not seem to be due to a differential ability of PC-hi/diss cells to adhere to intact $versus$ plasmin-treated fibronectin because cells adhered to both intact and cleaved fibronectin with similar efficiency (Figure W4A). The expression and functionality of the major

fibronectin receptor, $\alpha_5\beta_1$ integrin, were confirmed in PC-hi/diss cells by FACS analysis (Figure W4*B*), and function-blocking mAbs against α_5 and β_1 integrin subunits completely abrogated the binding of PC-hi/diss cells to intact as well as to plasmin-treated fibronectin (Figure W4*A*).

To validate the functional importance of fibronectin to invasion and escape of PC-hi/diss cells *in vivo*, intramesodermal microtumor assays

were performed in the presence of a function-blocking mAb preventing the interaction between $\alpha_5\beta_1$ integrin and its ligand, fibronectin. The P1D6 mAb, which specifically targets the α_5 integrin subunit, was used due to the known ability of the β_1 subunit to engage in interactions with multiple α subunits and the wide substrate repertoire of β_1 integrin complexes. Thus, PC-hi/diss microtumors were treated with anti-α_5
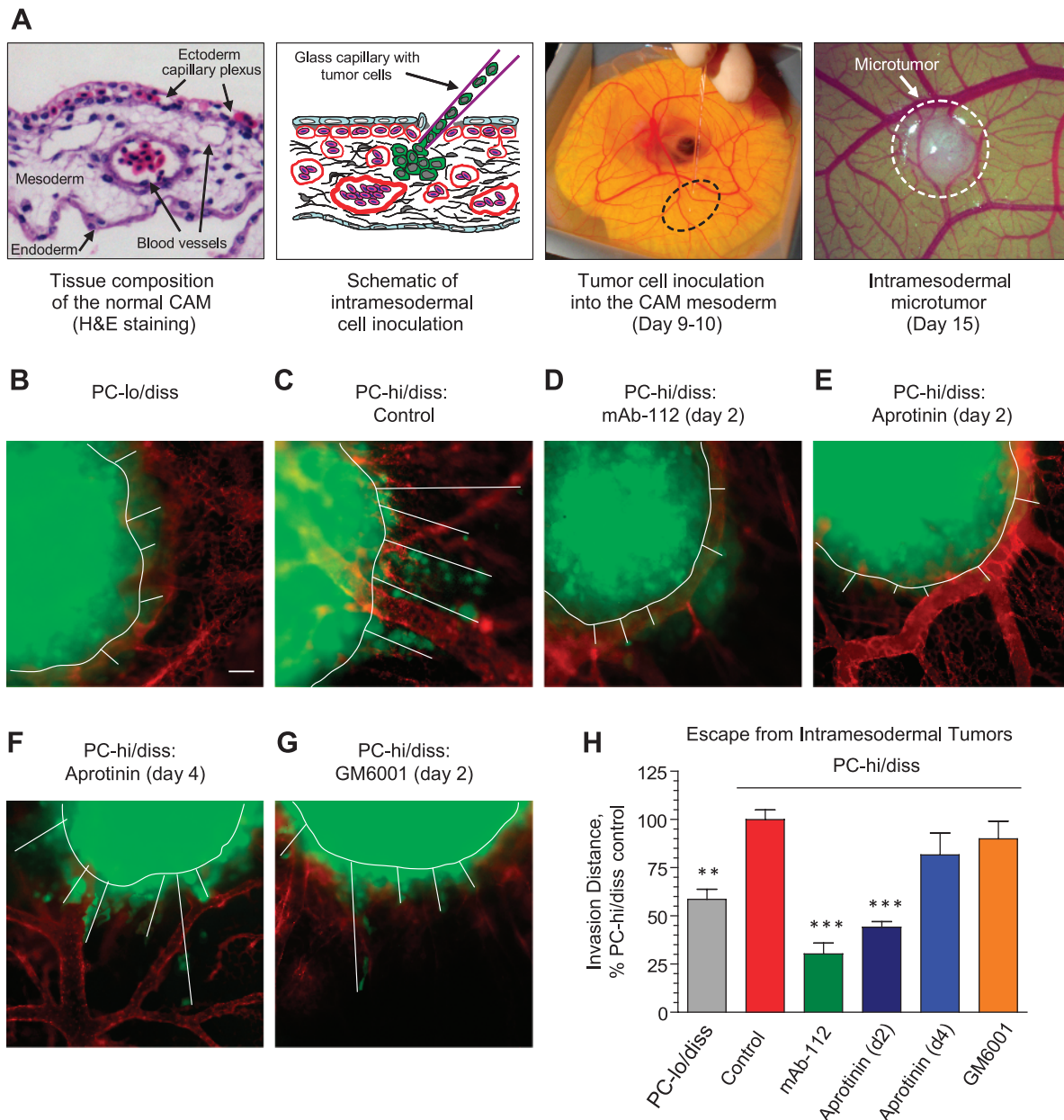

Figure 5. Activation of uPA facilitates early escape and invasion of PC-hi/diss tumor cells *in vivo*. (A) Left, Hematoxylin and eosin–stained section of the CAM depicting the endoderm, ectoderm capillary plexus, and mesoderm. Middle, Schematic and photographic depictions of tumor cell injection into the CAM mesoderm. Right, Intramesodermal microtumor developed 5 days after cell injection. (B-G) CellTracker Green–labeled PC-lo/diss and PC-hi/diss cells were intramesodermally injected into day 9 embryos. Developing PC-hi/diss microtumors were topically treated on day 2 (C-E) or day 4 (F) with control IgG (C), mAb-112 (D), aprotinin (E and F), or GM6001 (G). At day 6 after cell inoculations, microtumor-bearing embryos were injected with rhodamine-conjugated lectin, and portions of the CAM containing microtumors were excised and immediately imaged. Images were digitally acquired at an original magnification of ×100. Panels B to G depict representative microtumors from control and each of treatment groups. Microtumor borders and invasion distances of green fluorescent tumor cells are indicated by white lines. Scale bar, 50 μm. (H) Quantification of microtumor invasion was performed in digitally captured images by averaging the five longest distances of invasion for each microtumor. Data are presented as percent PC-hi/diss invasion in IgG control (100%), calculated for 10 to 16 individual microtumors per variable and are means ± SEM. **$P < .001$ and ***$P < .0001$, two-tailed Student's *t* test.
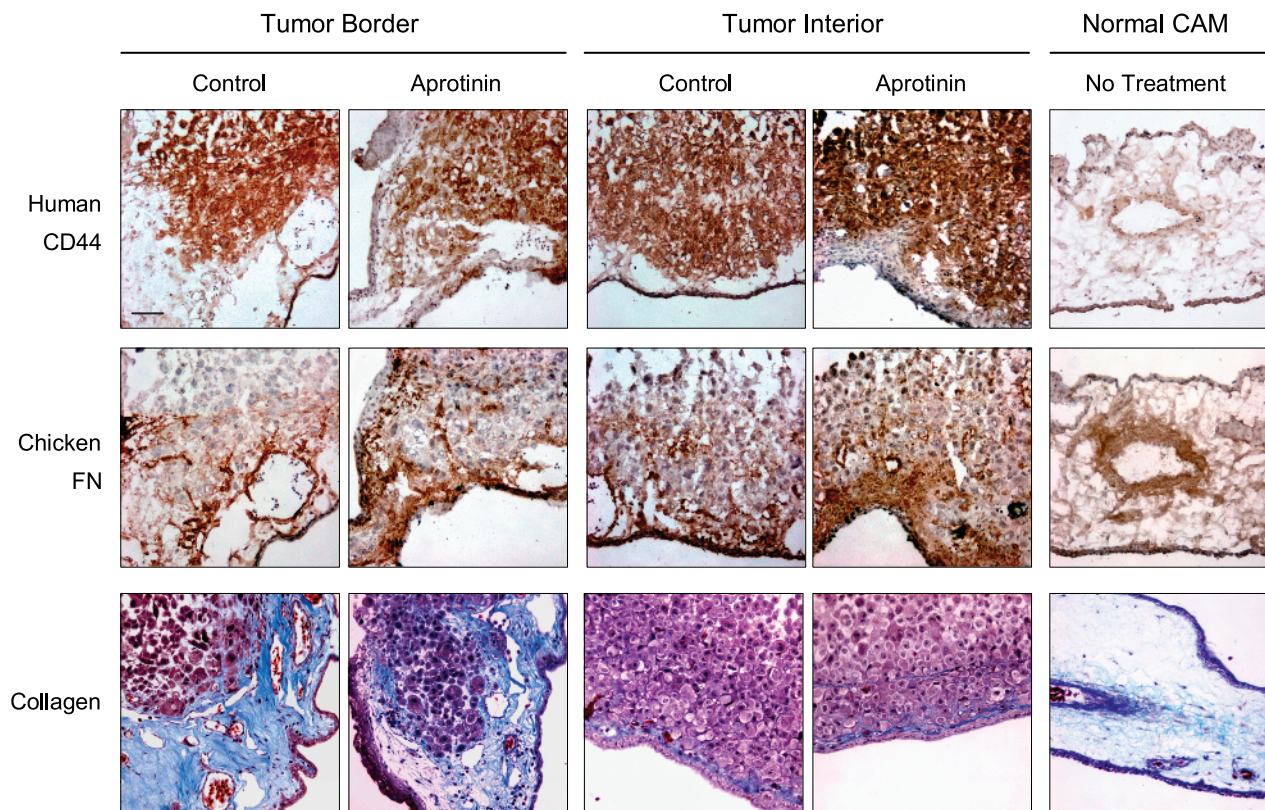
Figure 6. Immunohistochemical analysis of matrix collagen and fibronectin in PC-hi/diss primary CAM tumors. Consecutive tissue sections of frozen normal CAM and PC-hi/diss tumors, harvested from control embryos or embryos treated with aprotinin, were immunostained with antihuman CD44 mAb-29-7 to discriminate PC-hi/diss cells (dark brown, top panels) and mAb-B3/D6 to highlight avian fibronectin (middle panels). Sections from formalin-fixed paraffin-embedded tumors and normal CAM were stained with Masson trichrome to highlight collagen fibrils (bottom panels). Images were captured at an original magnification of ×200. Scale bar, 50 μm.

mAb on day 2 of microtumor development, and the extent of cell escape from the microtumors was analyzed and quantified by immunofluorescence microscopy at day 6 (Figure 8C). Preventing $\alpha_5\beta_1$ integrin–mediated cell interactions with fibronectin significantly reduced tumor cell invasion into the stroma surrounding the microtumors (Figure 8C, *bar graph*), thus validating the importance of an interaction between the escaping tumor cells with fibronectin. In conjunction with the above-described stimulation of PC-hi/diss migration by plasmin-treated fibronectin and the sensitivity of PC-hi/diss invasion to the plasmin inhibitor aprotinin, these results indicate that fibronectin may be a critical plasmin substrate involved in promoting the *in vivo* invasion, escape, and dissemination of PC-hi/diss cells.

Discussion

Herein, we have demonstrated the efficacy of preventing uPA activation as a strategy to inhibit intravasation and dissemination of human cancer cells by targeting the proteolysis-driven initial escape of cancer cells from the primary tumor. In a mouse prostate orthotopic metastasis model, the treatment of PC-hi/diss tumor-bearing mice with pro-uPA activation-blocking mAb-112 significantly inhibited local invasion and metastatic dissemination to secondary organs, including the brain, liver, and lungs. Furthermore, by using mAb-112 in a series of chick embryo models, we determined that pro-uPA activation triggers the onset of invasive escape of PC-hi/diss cells from primary tumors and that the specific targeting of pro-uPA activation was highly effective in reducing levels of spontaneous metastasis.

The serine protease inhibitor aprotinin also substantially inhibited escape, invasion, and dissemination in the chick embryo models. Aprotinin is a potent inhibitor of plasmin, a major feedback activator of pro-uPA as well as the key catalytic product generated by uPA-mediated activation of plasminogen [8]. Therefore, inhibition of PC-hi/diss spontaneous dissemination in the CAM model by aprotinin implicates the full uPA/plasmin system in the processes of metastatic spread. Continuous inhibition of plasmin by aprotinin in mammalian systems *in vivo*, however, is difficult to achieve. This could be due to the short half-life of Kunitz domain inhibitors in mammalian plasma, including a 150-minute half-life time for aprotinin [42,43], compared with antibody-based inhibitors, which can persist for days [44]. Furthermore, in some model systems, aprotinin treatment actually increased levels of experimental metastasis [45], indicating that the role of plasmin in the multistep metastatic cascade can be quite complex. Inhibition of plasmin activity may also facilitate metastasis by sustaining tumor-cell thrombi, potentially allowing for enhanced tumor cell survival in circulation and arrest at secondary sites [46,47]. These complex and seemingly contrasting effects of plasmin inhibition on tumor progression highlight the benefit of targeting the initial step in the tumor-initiated pro-uPA/uPA/plasminogen/plasmin cascade, that is, pro-uPA activation. Despite this complexity, the pronounced inhibitory effect of anti-uPA mAb-112 in reducing levels of spontaneous metastasis in both the murine and avian models suggests that specifically targeting pro-uPA activation at the early stages of tumor progression can provide an overall antimetastatic outcome. Our study, however, does not rule out a role for the uPA/plasmin cascade in the later events of cancer

dissemination such as vascular extravasation and tissue remodeling at secondary sites.

Consistent with the histologic appearance of the murine xenograft tumors, a dramatic reduction in formation of the invasive front was observed in PC-hi/diss primary CAM tumors treated with mAb-112 or aprotinin. This phenomenon was quantitatively evaluated in our newly developed intramesodermal tumor model, in which microtumors are formed directly in the mesoderm layer of the CAM, facilitating early invasion of tumor cells into the surrounding stroma and allowing for direct treatment and imaging of developing tumors and escaping cells. By treating the microtumors at early time points, we demonstrated that the initial PC-hi/diss cell escape was significantly inhibited by mAb-112 and aprotinin. Importantly, late treatments with aprotinin did not substantially inhibit invasion of escaping PC-hi/diss cells into the surrounding stroma. Together, these results indicate that uPA-generated plasmin is functionally important very early during tumor escape, possibly at the time when cancer cells initially break away from the bulk tumor mass. Interestingly, in the intramesodermal microtumor model, the MMP inhibitor GM6001

was ineffective in blocking the escape of PC-hi/diss carcinoma cells, in contrast to the significant inhibition by GM6001 of microtumor escape and invasion of mesenchymal HT-1080 fibrosarcoma cells (E.I.D., unpublished observations). These findings suggest that uPA/plasmin–mediated invasion of carcinoma cells may not involve the activation of MMPs by plasmin and indicate that initial escape and invasion in this specific model system is mainly mediated by MMP-independent, uPA/plasmin–governed mechanisms. However, critical roles of MMPs, such as MMP-1 and MMP-14, were demonstrated for carcinoma cell dissemination in other model systems, especially during late events of the metastatic cascade such as osteolytic metastasis of prostate and breast carcinoma cells to the bone [48,49].

The uPA-generated plasmin has broad substrate specificity, and multiple plasmin substrates may be involved in facilitating early tumor cell escape, invasion, and dissemination. We speculated that some of the plasmin ECM substrates may accumulate within and at the stromal border of developing PC-hi/diss tumors and that plasmin-mediated cleavage of such substrates might stimulate migration or facilitate invasion and escape of primary tumor cells. Among natural plasmin targets,
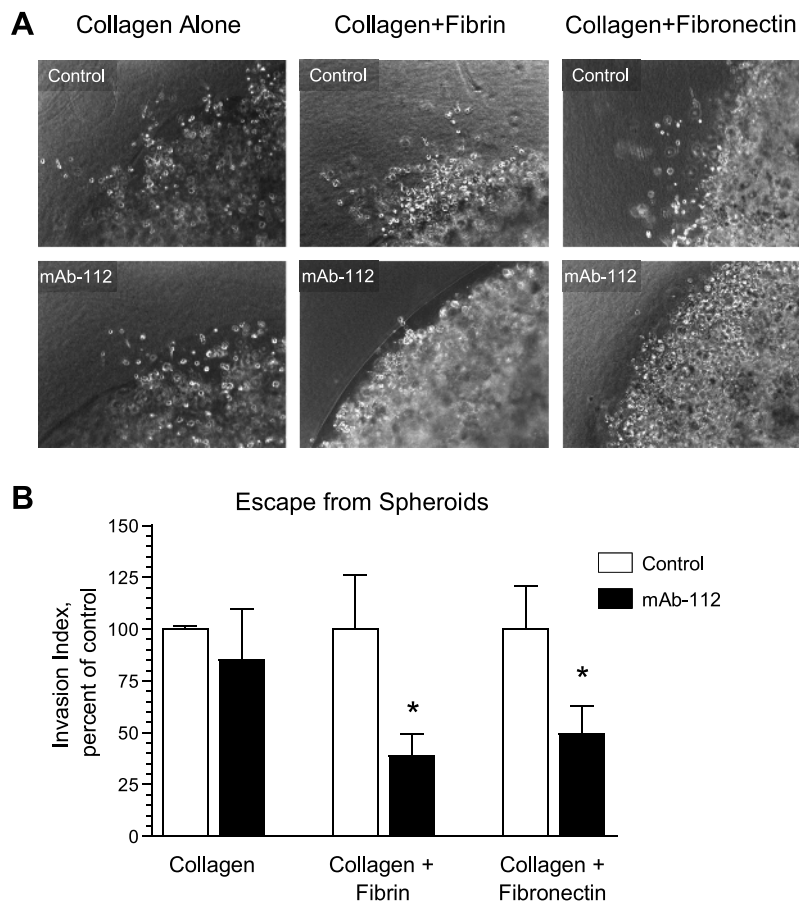

Figure 7. uPA activation promotes invasion of three-dimensional fibrillar collagen matrices supplemented with the plasmin substrates fibronectin and fibrin. (A) Collagen droplets containing PC-hi/diss cells were incorporated into three-dimensional gels containing collagen I only, a mixture of collagen I and thrombin-clotted fibrin, or a mixture of collagen I and fibronectin, prepared as described in the Materials and Methods section. All outer gels were supplemented with EGF to induce chemotactic invasion from inner cell–containing collagen droplets. Gels were overlaid with AIM-V medium supplemented with control IgG or mAb-112. Medium was replaced every 3 to 4 days. After 10 days of incubation, digital images were captured at an original magnification of ×100. (B) An invasion index was calculated from individual images by multiplying the individual lengths of invasion by the number of tumor cells invaded beyond the original boundaries of collagen droplets. At least six images at an original magnification of ×100 were analyzed per variable per experiment. Data are presented as percent invasion in control (100%) and are the pooled means ± SEM from two to three experiments. *P < .05, one-tailed Student's t test.
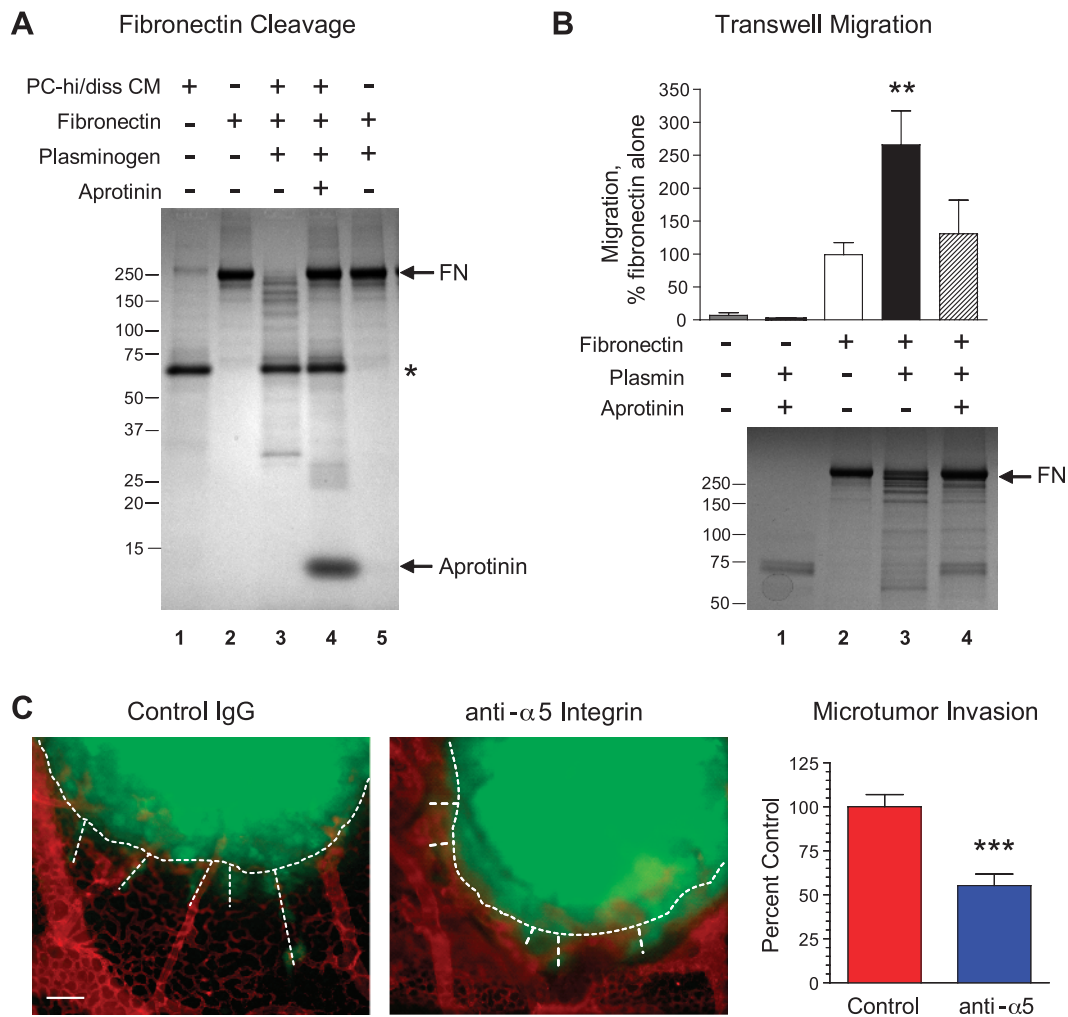
Figure 8. Cleavage of fibronectin by uPA-generated plasmin as a potential mechanism of enhanced invasion and escape of PC-hi/diss cells from primary tumors. (A) Cleavage of fibronectin by active plasmin generated by PC-hi/diss uPA. Fibronectin (FN) was incubated in the presence or absence of PC-hi/diss CM, plasminogen, and aprotinin for 18 hours at 37°C. Samples were boiled in SDS buffer and separated by SDS-PAGE under nonreducing conditions. Gels were stained with Coomassie blue dye. The position of intact fibronectin (lanes 2, 4, and 5) is indicated on the right. Fibronectin cleavage products were produced in the presence of PC-hi/diss CM and plasminogen (lane 3) but not in the presence of aprotinin (lane 4) or plasminogen alone (lane 5), suggesting uPA-generated plasmin activity. *Asterisk* points to a major protein component of PC-hi/diss CM, which was resistant to fibronectin-cleaving activity of the generated serine proteases (lane 3), further indicating the specificity of fibronectin cleavage by the uPA-generated plasmin. The positions of the molecular weight markers (kDa) are indicated on the left. (B) Haptotactic migration of PC-hi/diss cells toward plasmin-cleaved fibronectin. The undersides of 8-μm pore Transwells were coated with fibronectin and incubated with plasmin in the presence or absence of aprotinin. After incubation, Transwells were washed and placed in the wells filled with SF-DMEM. PC-hi/diss cells were placed into the inserts in SF-DMEM and the cells that had migrated into the outer chambers were counted at 18 to 24 hours (bar graph). Data are presented as percent migration toward nontreated fibronectin (100%) and are means ± SEM calculated from three independent experiments, each performed in duplicate. **$P < .01$, two-tailed Student's t test. Fibronectin cleavage by plasmin and inhibition of this cleavage by aprotinin were confirmed in parallel reactions by presence and absence of fibronectin cleavage products in Coomassie-stained gels (bottom). The positions of the molecular weight markers (kDa) are indicated on the right. (C) CellTracker Green–labeled PC-hi/diss cells were injected into the CAM mesoderm of day 9 embryos. The microtumors were topically treated with anti–α_5 integrin antibody on day 2 after cell injections. At day 6, the embryos were injected with rhodamine-conjugated lectin, and portions of the CAM containing microtumors were imaged by fluorescence microscopy. Dashed lines outline microtumor borders and highlight trails of escaping green fluorescent tumor cells in images captured at an original magnification of ×100. Scale bar, 50 μm. Bar graph, The invasion index for each variable was calculated as described in the Materials and Methods section from a total of 22 to 24 individual microtumors developed in five embryos. Data are presented as means ± SEM of the percent of invasion in the control-treated embryos (100%). ***$P < .0001$, two-tailed Student's t test.

fibrin is often considered to be the most physiologically important plasmin substrate. However, extensive fibrin deposition was not observed in the PC-hi/diss tumors and was not enhanced by aprotinin treatment, consistent with previous reports demonstrating the lack of immunohistochemically detectable changes in fibrin deposition within tumors developing in plasminogen knockout *versus* control mice, despite fibrin(ogen) being a critical substrate promoting plasmin-dependent tumor growth and progression [50].

Plasmin-mediated protein modifications have also been implicated during adipocyte differentiation, when plasmin exerts its effects by cleaving a nonfibrin substrate, namely fibronectin [51]. Limited cleavage of fibronectin by uPA and plasmin has been previously shown in a model system using avian fibroblasts [17]. Furthermore, fibronectin itself and fibronectin-integrin interactions have long been linked to tumor development and metastasis [19,52–54]. A pronounced accumulation of fibronectin within and around the PC-hi/diss tumors was observed *in vivo* in the avian xenograft tumor model, especially in aprotinin-treated tumors. We suggested that plasmin-mediated fibronectin remodeling, mediated by tumor cell uPA, might mechanistically contribute to PC-hi/diss initial escape and subsequent metastasis. To validate this notion, we first verified that fibronectin fragments are generated after treatment with the mixture of plasminogen and uPA-containing tumor cell CM as a source of plasminogen activator. Supporting a role for plasmin-modified fibronectin in PC-hi/diss migration, the limited proteolysis of fibronectin by plasmin substantially enhanced its capacity to induce cell migration *in vitro*. Accumulation of fibronectin in aprotinin-treated tumors further validated that proteolytic cleavage of matrix fibronectin by serine proteases, including plasmin, occurs *in vivo* in the tumor-associated stroma. In addition to widespread proteolytic remodeling and pathway clearing of the tumor tissue ECM, it is likely that the plasmin-cleaved fibronectin, through interactions with its cell surface receptor, can facilitate tumor cell escape and invasion *in vivo*, as evidenced by the inhibitory effects of blocking $\alpha_5\beta_1$ integrin functions on escape of PC-hi/diss cells in the intramesodermal microtumor model. Altogether, our findings point to pro-uPA activation as a critical process during early stages of cancer cell dissemination and suggest that fibronectin may be a critical target of the uPA/plasmin proteolytic cascade involved in the initial invasive escape of carcinoma cells.

Acknowledgments

References

[1] Duffy MJ, McGowan PM, and Gallagher WM (2008). Cancer invasion and metastasis: changing views. *J Pathol* **214**, 283–293.

[2] Kessenbrock K, Plaks V, and Werb Z (2010). Matrix metalloproteinases: regulators of the tumor microenvironment. *Cell* **141**, 52–67.

[3] Usher PA, Thomsen OF, Iversen P, Johnsen M, Brunner N, Hoyer-Hansen G, Andreasen P, Dano K, and Nielsen BS (2005). Expression of urokinase plasminogen activator, its receptor and type-1 inhibitor in malignant and benign prostate tissue. *Int J Cancer* **113**, 870–880.

[4] Cozzi PJ, Wang J, Delprado W, Madigan MC, Fairy S, Russell PJ, and Li Y (2006). Evaluation of urokinase plasminogen activator and its receptor in different grades of human prostate cancer. *Hum Pathol* **37**, 1442–1451.

[5] Shariat SF, Roehrborn CG, McConnell JD, Park S, Alam N, Wheeler TM, and Slawin KM (2007). Association of the circulating levels of the urokinase system of plasminogen activation with the presence of prostate cancer and invasion, progression, and metastasis. *J Clin Oncol* **25**, 349–355.

[6] Li Y and Cozzi PJ (2007). Targeting uPA/uPAR in prostate cancer. *Cancer Treat Rev* **33**, 521–527.

[7] Andreasen PA, Egelund R, and Petersen HH (2000). The plasminogen activation system in tumor growth, invasion, and metastasis. *Cell Mol Life Sci* **57**, 25–40.

[8] Behrendt N, List K, Andreasen PA, and Dano K (2003). The pro-urokinase plasminogen-activation system in the presence of serpin-type inhibitors and the urokinase receptor: rescue of activity through reciprocal pro-enzyme activation. *Biochem J* **371**, 277–287.

[9] Dano K, Behrendt N, Hoyer-Hansen G, Johnsen M, Lund LR, Ploug M, and Romer J (2005). Plasminogen activation and cancer. *Thromb Haemost* **93**, 676–681.

[10] Vincenza Carriero M, Franco P, Vocca I, Alfano D, Longanesi-Cattani I, Bifulco K, Mancini A, Caputi M, and Stoppelli MP (2009). Structure, function and antagonists of urokinase-type plasminogen activator. *Front Biosci* **14**, 3782–3794.

[11] Blasi F and Carmeliet P (2002). uPAR: a versatile signalling orchestrator. *Nat Rev Mol Cell Biol* **3**, 932–943.

[12] Binder BR, Mihaly J, and Prager GW (2007). uPAR-uPA–PAI-1 interactions and signaling: a vascular biologist's view. *Thromb Haemost* **97**, 336–342.

[13] Ellis V, Behrendt N, and Dano K (1991). Plasminogen activation by receptor-bound urokinase. A kinetic study with both cell-associated and isolated receptor. *J Biol Chem* **266**, 12752–12758.

[14] Hajjar KA, Jacovina AT, and Chacko J (1994). An endothelial cell receptor for plasminogen/tissue plasminogen activator. I. Identity with annexin II. *J Biol Chem* **269**, 21191–21197.

[15] Andronicos NM, Chen EI, Baik N, Bai H, Parmer CM, Kiosses WB, Kamps MP, Yates JR III, Parmer RJ, and Miles LA (2010). Proteomics-based discovery of a novel, structurally unique, and developmentally regulated plasminogen receptor, Plg-RKT, a major regulator of cell surface plasminogen activation. *Blood* **115**, 1319–1330.

[16] Myohanen H and Vaheri A (2004). Regulation and interactions in the activation of cell-associated plasminogen. *Cell Mol Life Sci* **61**, 2840–2858.

[17] Quigley JP, Gold LI, Schwimmer R, and Sullivan LM (1987). Limited cleavage of cellular fibronectin by plasminogen activator purified from transformed cells. *Proc Natl Acad Sci USA* **84**, 2776–2780.

[18] Goldfinger LE, Stack MS, and Jones JC (1998). Processing of laminin-5 and its functional consequences: role of plasmin and tissue-type plasminogen activator. *J Cell Biol* **141**, 255–265.

[19] Pankov R and Yamada KM (2002). Fibronectin at a glance. *J Cell Sci* **115**, 3861–3863.

[20] Murphy G, Stanton H, Cowell S, Butler G, Knauper V, Atkinson S, and Gavrilovic J (1999). Mechanisms for pro matrix metalloproteinase activation. *APMIS* **107**, 38–44.

[21] Ramos-DeSimone N, Hahn-Dantona E, Sipley J, Nagase H, French DL, and Quigley JP (1999). Activation of matrix metalloproteinase-9 (MMP-9) via a converging plasmin/stromelysin-1 cascade enhances tumor cell invasion. *J Biol Chem* **274**, 13066–13076.

[22] Sheng S (2001). The urokinase-type plasminogen activator system in prostate cancer metastasis. *Cancer Metastasis Rev* **20**, 287–296.

[23] Sidenius N and Blasi F (2003). The urokinase plasminogen activator system in cancer: recent advances and implication for prognosis and therapy. *Cancer Metastasis Rev* **22**, 205–222.

[24] Rockway TW, Nienaber V, and Giranda VL (2002). Inhibitors of the protease domain of urokinase-type plasminogen activator. *Curr Pharm Des* **8**, 2541–2558.

[25] Pulukuri SM, Gondi CS, Lakka SS, Jutla A, Estes N, Gujrati M, and Rao JS (2005). RNA interference–directed knockdown of urokinase plasminogen activator and urokinase plasminogen activator receptor inhibits prostate cancer cell invasion, survival, and tumorigenicity *in vivo*. *J Biol Chem* **280**, 36529–36540.

[26] Pulukuri SM, Estes N, Patel J, and Rao JS (2007). Demethylation-linked activation of urokinase plasminogen activator is involved in progression of prostate cancer. *Cancer Res* **67**, 930–939.

[27] Dong Z, Saliganan AD, Meng H, Nabha SM, Sabbota AL, Sheng S, Bonfil RD, and Cher ML (2008). Prostate cancer cell–derived urokinase-type plasminogen activator contributes to intraosseous tumor growth and bone turnover. *Neoplasia* **10**, 439–449.

[28] Pulukuri SM and Rao JS (2007). Small interfering RNA directed reversal of urokinase plasminogen activator demethylation inhibits prostate tumor growth and metastasis. *Cancer Res* **67**, 6637–6646.

[29] Bugge TH, Kombrinck KW, Flick MJ, Daugherty CC, Danton MJ, and Degen JL (1996). Loss of fibrinogen rescues mice from the pleiotropic effects of plasminogen deficiency. *Cell* **87**, 709–719.

[30] Bugge TH, Lund LR, Kombrinck KK, Nielsen BS, Holmback K, Drew AF, Flick MJ, Witte DP, Dano K, and Degen JL (1998). Reduced metastasis of Polyoma virus middle T antigen–induced mammary cancer in plasminogen-deficient mice. *Oncogene* **16**, 3097–3104.

[31] Almholt K, Lund LR, Rygaard J, Nielsen BS, Dano K, Romer J, and Johnsen M (2005). Reduced metastasis of transgenic mammary cancer in urokinase-deficient mice. *Int J Cancer* **113**, 525–532.

[32] Madsen MA, Deryugina EI, Niessen S, Cravatt BF, and Quigley JP (2006). Activity-based protein profiling implicates urokinase activation as a key step in human fibrosarcoma intravasation. *J Biol Chem* **281**, 15997–16005.

[33] Blouse GE, Botkjaer KA, Deryugina E, Byszuk AA, Jensen JM, Mortensen KK, Quigley JP, and Andreasen PA (2009). A novel mode of intervention with serine protease activity: targeting zymogen activation. *J Biol Chem* **284**, 4647–4657.

[34] Conn EM, Botkjaer KA, Kupriyanova TA, Andreasen PA, Deryugina EI, and Quigley JP (2009). Comparative analysis of metastasis variants derived from human prostate carcinoma cells: roles in intravasation of VEGF-mediated angiogenesis and uPA-mediated invasion. *Am J Pathol* **175**, 1638–1652.

[35] Deryugina EI, Zijlstra A, Partridge JJ, Kupriyanova TA, Madsen MA, Papagiannakopoulos T, and Quigley JP (2005). Unexpected effect of matrix metalloproteinase down-regulation on vascular intravasation and metastasis of human fibrosarcoma cells selected *in vivo* for high rates of dissemination. *Cancer Res* **65**, 10959–10969.

[36] Zijlstra A, Mellor R, Panzarella G, Aimes RT, Hooper JD, Marchenko ND, and Quigley JP (2002). A quantitative analysis of rate-limiting steps in the metastatic cascade using human-specific real-time polymerase chain reaction. *Cancer Res* **62**, 7083–7092.

[37] Moran P, Li W, Fan B, Vij R, Eigenbrot C, and Kirchhofer D (2006). Pro–urokinase-type plasminogen activator is a substrate for hepsin. *J Biol Chem* **281**, 30439–30446.

[38] Lee SL, Dickson RB, and Lin CY (2000). Activation of hepatocyte growth factor and urokinase/plasminogen activator by matriptase, an epithelial membrane serine protease. *J Biol Chem* **275**, 36720–36725.

[39] Takeuchi T, Harris JL, Huang W, Yan KW, Coughlin SR, and Craik CS (2000). Cellular localization of membrane-type serine protease 1 and identification of protease-activated receptor-2 and single-chain urokinase-type plasminogen activator as substrates. *J Biol Chem* **275**, 26333–26342.

[40] Pilcher BK, Dumin JA, Sudbeck BD, Krane SM, Welgus HG, and Parks WC (1997). The activity of collagenase-1 is required for keratinocyte migration on a type I collagen matrix. *J Cell Biol* **137**, 1445–1457.

[41] Zijlstra A, Aimes RT, Zhu D, Regazzoni K, Kupriyanova T, Seandel M, Deryugina EI, and Quigley JP (2004). Collagenolysis-dependent angiogenesis mediated by matrix metalloproteinase-13 (collagenase-3). *J Biol Chem* **279**, 27633–27645.

[42] Janssens M, Joris J, David JL, Lemaire R, and Lamy M (1994). High-dose aprotinin reduces blood loss in patients undergoing total hip replacement surgery. *Anesthesiology* **80**, 23–29.

[43] Stassen JM, Lambeir AM, Matthyssens G, Ripka WC, Nystrom A, Sixma JJ, and Vermylen J (1995). Characterisation of a novel series of aprotinin-derived anticoagulants. I. *In vitro* and pharmacological properties. *Thromb Haemost* **74**, 646–654.

[44] Kontermann RE (2009). Strategies to extend plasma half-lives of recombinant antibodies. *BioDrugs* **23**, 93–109.

[45] Kirstein JM, Graham KC, Mackenzie LT, Johnston DE, Martin LJ, Tuck AB, MacDonald IC, and Chambers AF (2009). Effect of anti-fibrinolytic therapy on experimental melanoma metastasis. *Clin Exp Metastasis* **26**, 121–131.

[46] Erpenbeck L and Schon MP (2010). Deadly allies: the fatal interplay between platelets and metastasizing cancer cells. *Blood* **115**, 3427–3436.

[47] Gay LJ and Felding-Habermann B (2011). Contribution of platelets to tumour metastasis. *Nat Rev Cancer* **11**, 123–134.

[48] Sabbota AL, Kim HR, Zhe X, Fridman R, Bonfil RD, and Cher ML (2010). Shedding of RANKL by tumor-associated MT1-MMP activates Src-dependent prostate cancer cell migration. *Cancer Res* **70**, 5558–5566.

[49] Lu X, Wang Q, Hu G, Van Poznak C, Fleisher M, Reiss M, Massague J, and Kang Y (2009). ADAMTS1 and MMP1 proteolytically engage EGF-like ligands in an osteolytic signaling cascade for bone metastasis. *Genes Dev* **23**, 1882–1894.

[50] Palumbo JS, Talmage KE, Liu H, La Jeunesse CM, Witte DP, and Degen JL (2003). Plasminogen supports tumor growth through a fibrinogen-dependent mechanism linked to vascular patency. *Blood* **102**, 2819–2827.

[51] Selvarajan S, Lund LR, Takeuchi T, Craik CS, and Werb Z (2001). A plasma kallikrein-dependent plasminogen cascade required for adipocyte differentiation. *Nat Cell Biol* **3**, 267–275.

[52] Akiyama SK, Olden K, and Yamada KM (1995). Fibronectin and integrins in invasion and metastasis. *Cancer Metastasis Rev* **14**, 173–189.

[53] Hynes RO (1999). Fibronectins. In *Guidebook to the Extracellular Matrix, Anchor and Adhesion Proteins.* T Kreis and R Vale (Eds). Oxford University Press, New York, NY. pp. 422–425.

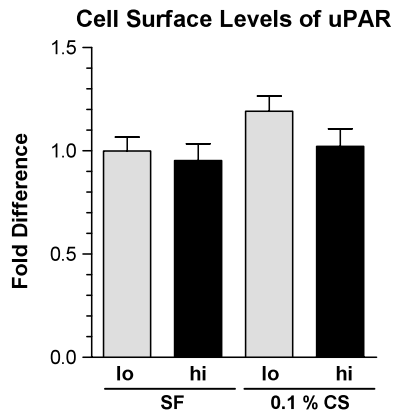[54] Ruoslahti E (2003). RGD story: a personal account. A landmark essay. *Matrix Biol* **22**, 459–465.

Cell Surface Levels of uPAR

Figure W1. Levels of uPAR at the cell surface of PC-lo/diss and PC-hi/diss cells. Cell surface levels of uPAR on PC-lo/diss (gray bars) and PC-hi/diss (black bars) monolayers were determined using whole-cell ELISA PC-lo/diss and PC-hi/diss cells were seeded at equal density into 96-well plates precoated with 10 μg/ml type I collagen in serum-free AIM-V medium (Gibco, Grand Island, NY) or AIM-V medium supplemented with 0.1% chicken serum. After 24 hours, the cells were washed, fixed in 2% paraformaldehyde, and blocked with 1% bovine serum albumin in PBS–0.05% Tween 20. Primary mAb 3936 against uPAR (American Diagnostica Inc., Stamford, CT) was added at 2 μg/ml in blocking solution for 1 hour at room temperature, followed by incubation with anti-mouse HRP (Bio-Rad) at 0.5 μg/ml for 1 hour. After washing, ABTS substrate was added, and the optical density was determined at 405 nm. The background readings from control IgG wells were subtracted from the data. Fold differences in uPAR levels were calculated in comparison to PC-lo/diss cells incubated without serum (100%). Data are presented as means ± SEM from triplicate wells.
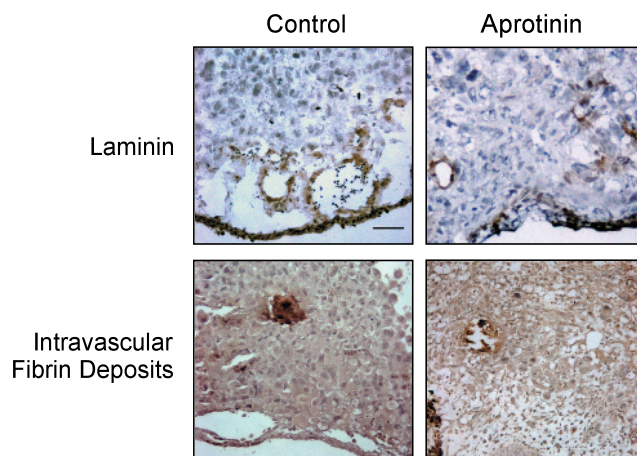

Figure W2. Immunohistochemical analysis of laminin and fibrin within primary CAM tumors. Frozen tissue sections from PC-hi/diss tumors, treated with aprotinin or buffer (vehicle control), were immunostained with mAb ″31 or 31-2″ recognizing avian laminin (top). Positive laminin immunostaining (brown) was associated with medium-to-large blood vessels in both control and aprotinin-treated tumors. Formalin-fixed paraffin-embedded sections were stained with anti-fibrin antibody to visualize fibrin clots, which were rare in both control and aprotinin-treated tumors and were only observed intravascularly (bottom). Images were captured at an original magnification of ×200. Scale bar, 25 μm.
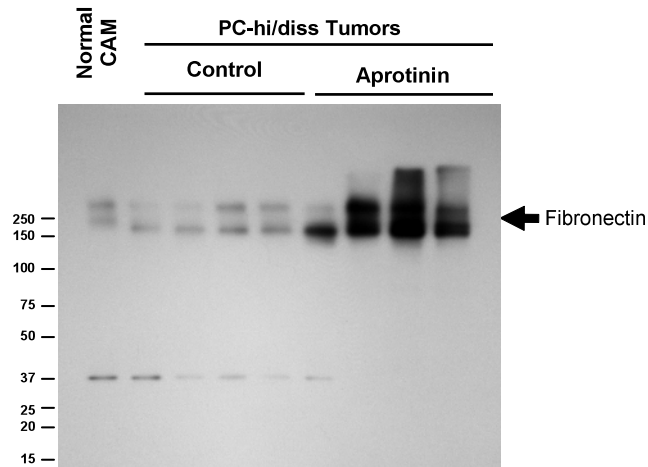
Figure W3. Accumulation of fibronectin in aprotinin-treated PC-hi/diss CAM tumors. Normal CAM was harvested from the embryos on day 16 of incubation. PC-hi/diss primary tumors, treated with aprotinin or buffer control, were harvested 6 days after cell grafting on the CAM. Harvested tissues were washed and lysed. Lysate samples containing 20 μg of protein were separated by SDS-PAGE under nonreducing conditions, transferred to a membrane support, and probed with mAb–B3/D6 to detect avian fibronectin. The positions of molecular weight markers (kDa) are indicated on the left.
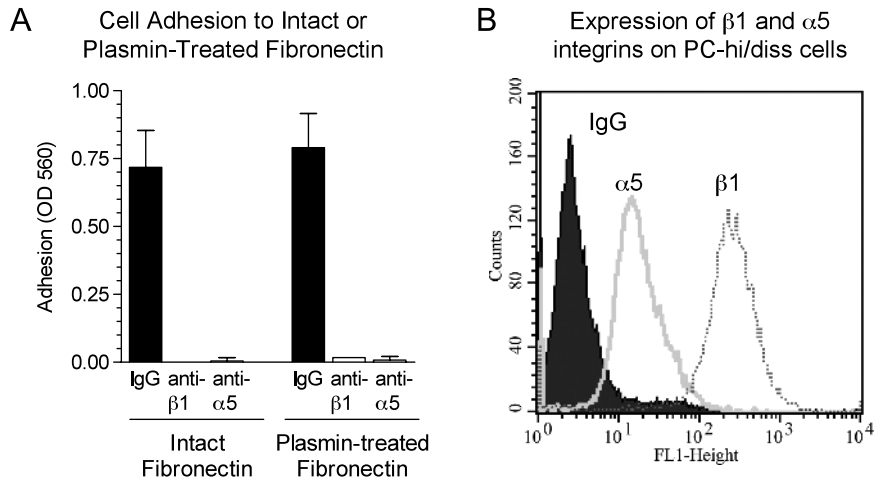

Figure W4. (A) PC-hi/diss cells express functional $\alpha_5\beta_1$ integrin, mediating adhesion to fibronectin. Multiwell plates were coated for 1.5 hours with 10 μg/ml fibronectin, which was left intact or treated with 40 nM plasmin overnight at 37°C. After plate washing and blocking with 1% bovine serum albumin, PC-hi/diss cells were allowed to adhere for 45 minutes in the presence of function-blocking antibodies against the β_1 or α_5 integrin subunits. Nonadherent cells were washed out, and adherent cells were fixed and stained with crystal violet. Cell-incorporated dye was extracted, and absorption, proportional to the cell number, was measured at 560 nm. Data are presented as means ± SEM of absorbance from triplicate wells. (B) Cell surface expression of the α_5 and β_1 integrin subunits in PC-hi/diss cells was determined by FACS analysis in comparison to control IgG. The cells were incubated for 1 hour with 3 μg/ml primary antibodies at 4°C, followed by incubation with fluorescein isothiocyanate–conjugated secondary anti-mouse antibodies (Sigma).